Article:
Alcott, LJ, Mills, BJW orcid.org/0000-0002-9141-0931, Bekker, A et al. (1 more author) (2022) Earth's Great Oxidation Event facilitated by the rise of sedimentary phosphorus recycling. Nature Geoscience, 15 (3). pp. 210-215. ISSN 1752-0894

https://doi.org/10.1038/s41561-022-00906-5

Supplementary Information

Geological and stratigraphic context

The Kaapvaal craton covers more than 10^6 km^2 with a general trend of older to younger successions from east to west, with the most ancient terranes being formed at ~3.6 Ga[1]. Continued cratonic development is viewed as being driven by a period of continental growth (starting at *c.* 3.1 Ga) until the final craton stabilization at approximately 2.6 Ga[1]. This period led to extensive development of depositional basins, including the two Neoarchean – Paleoproterozoic structural sub-basins considered in this study, the Transvaal and Griqualand West sub-basins[2]. Both structural sub-basins preserve the Transvaal Supergroup, and were parts of a single depositional basin.

The Griqualand West sub-basin preserves the Ghaap Group (Figure S1), which correlates to the Chuniespoort Group of the Transvaal sub-basin[2]. The Ghaap Group is considered to have undergone minimal metamorphism (sub-greenschist facies) and contains four subgroups[3]. The oldest, the Schmidtsdrif Subgroup, unconformably overlies the Ventersdorp Supergroup and contains tidal sandstones overlain by shallow-marine carbonates. The uppermost Schmidtsdrif Subgroup includes the Lokamonna Formation with deeper-water siliciclastic mudstones[4]. The Campbellrand Subgroup is dated at ~2.6 – 2.5 Ga[5,6] and records the development of an extensive carbonate platform, which was ultimately drowned to allow deposition of the Asbestos Hills Subgroup iron formations[3]. A switch from chemical sedimentation to siliciclastic-chemical deposition defines the transition from the siderite and greenalite-rich Griquatown Iron Formation of the Asbestos Hills Subgroup, to the Koegas Subgroup, which consists of several transgressive-regressive cycles deposited in a delta-submarine fan depositional setting[7]. This study primarily focuses on the Campbellrand, Asbestos Hills, and Koegas subgroups. We briefly describe the stratigraphy and sedimentology of these three subgroups here (Figure S2), with a more extensive reviews in refs 4 and 7.

The carbonate platform of the Campbellrand Subgroup includes the Monteville, Nauga, and Klein Naute formations. The Monteville Formation consists of metre-scale parasequences starting with slope dolostones, and progressing grades into dolograinstones and microbialites[4]. Underlying the

Monteville Formation, the Lokamonna Formation is dated at ~2650 Ma[8] and consists of mixed shallow-marine carbonate-siliciclastics[4]. The Nauga Formation has been informally divided into lower and upper units. The lower Nauga Formation was also deposited on a slope and contains both microbialites and reworked carbonate lithologies. The upper and lower Nauga formations are separated by the Kamden Member. The upper unit was also deposited in a slope setting with a deepening and/or higher input of fine-grained detrital material[4]. The Klein Naute Formation contains massive and laminated siliciclastic mudstone with abundant diagenetic pyrite and chert nodules[4], and is dated at ~2549 ± 7 Ma[5].

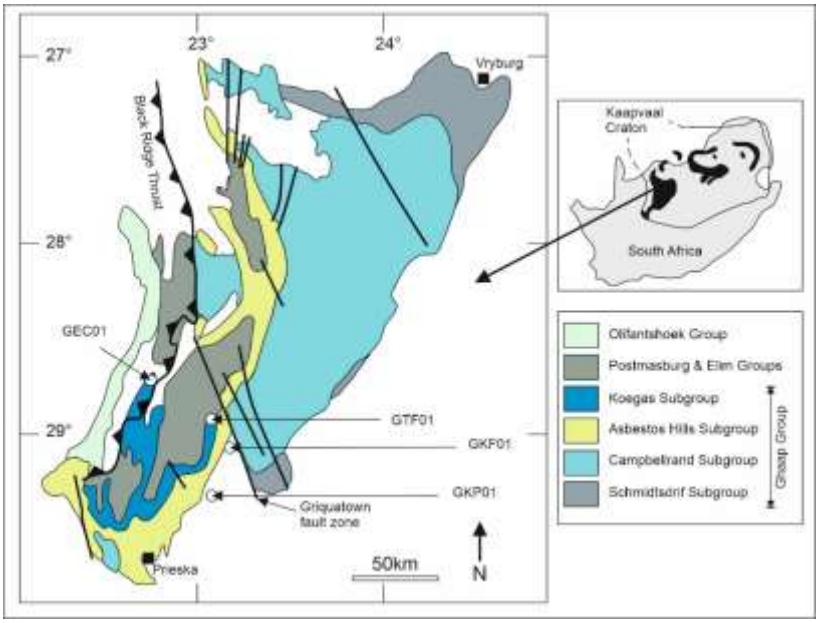

Figure S1. Geological map of the Griqualand West sub-basin. Location of the four studied drill cores indicated by white dots. Inset map shows outcrop area of both the Griqualand West and Transvaal sub-basins, in addition to a generalised stratigraphy of the Ghaap Group.

The Asbestos Hills Subgroup (~2.45 Ga[9,10]) conformably overlies the Campbellrand Subgroup and primarily includes iron formation and chert sediments (<1,000 m thick[11]). The initial drowning of the Campbellrand carbonate platform led to deposition of banded iron formation and chert sediments of the Kuruman Iron Formation, leading into the granular iron formation of the Griquatown Iron Formation[11]. The Kuruman Iron Formation includes magnetite BIF and sideritic chert, and records persistent BIF deposition[4] at 2,484.6 ± 0.34 Ma[12]. The magnetite-rich BIF dominantly consists of

magnetite, with more minor contributions from siderite and hematite, whereas the sideritic chert is rich in siderite, with stilpnomeline rhythmites[4]. Following the Kuruman Iron Formation, the Griquatown Iron Formation consists of banded and granular iron formation sediments deposited in a relatively shallow-marine environment with storm and wave influence[11]. The Griquatown Iron Formation is poorly dated at ~2432 ± 31 Ma[9].

The Koegas Subgroup comprises intercalated siliciclastic and chemically precipitated iron-rich sediments[7] and is older than the overlying Ongeluk Formation volcanics (2426 ± 3 Ma[13]). At the base of the Koegas Subgroup, the Pannetjie Formation contains an upward-coarsening mudstone to greywacke succession that is terminated by the Doradale Iron Formation, which marks the transition back to chemical precipitates[7]. Continued shallowing from the Doradale Iron Formation defines the transition to the Naragas Formation, with a greater proportion of sandstone towards the northeast as opposed to mudstone in the SW[14]. The third depositional cycle comprises the Heynskop Formation, which includes iron-rich lithologies, shallowing towards coarser siliciclastic units upsection[7]. The overlying Rooinekke Formation predominantly comprises banded iron formation and stromatolitic bioherms, which are almost exclusively limestone[7]. The Nelani Formation is only developed in the distal drill core sampled here (GEC01). The Koegas Subgroup contains modest manganese concentrations in carbonate phases, the initial genesis of which has been linked to the development of oxygen oases[15]. The Makganyene Formation overlies the Koegas Subgroup and represents the oldest of the low-latitude glaciations associated with the Great Oxidation Event[13]. The contact between the Makganyene Formation and Koegas Subgroup is considered to be erosional, but the missing period of time has recently been reduced by up to 200 Myrs[13].

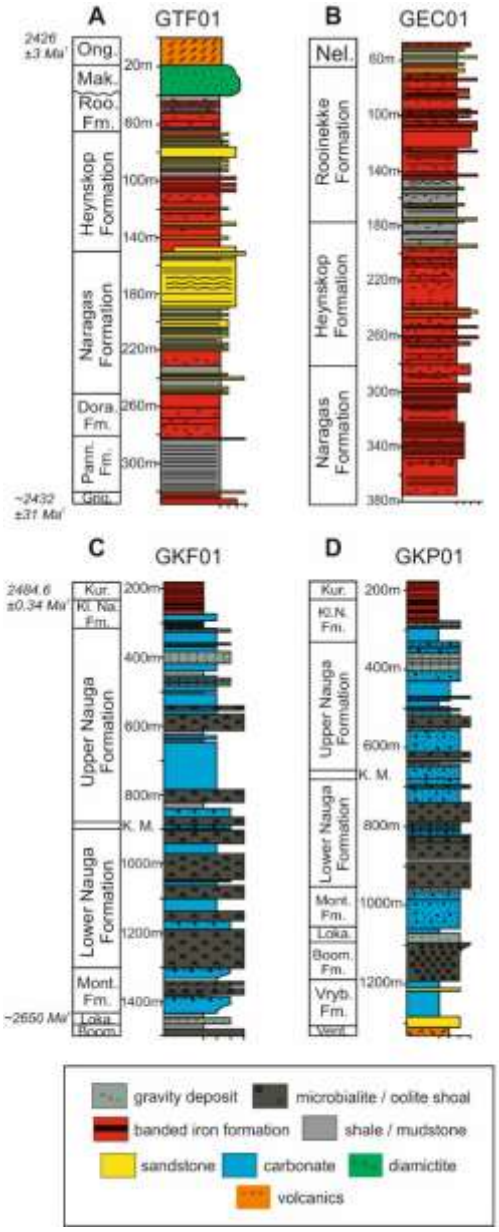

Figure S2. Stratigraphic columns of the four studied drill cores (Schröder et al., 2006[4]; 2011[7]). (A) GTF01 drill core. (B) GEC01 drill core. (C) GKF01 drill core. (D) GKP01 drill core. Abbreviations for formations: Ong. – Ongeluk Formation; Mak. – Makganyene Formation; Roo. – Rooinekke Formation; Dora. – Doredale Formation; Pann. – Pannetjie Formation; Griq. – Griquatown Iron Formation; Nel. – Nelani Formation; Dwyka. – Dwyka Formation; Kur. – Kuruman Iron Formation; Kl. Na. – Klein Naute Formation; K. – Kamden Member; Mont. – Monteville Formation; Loka. – Lokamonna Formation; Boom. – Boompaas Formation; Vryb. – Vryburg Formation; Vent. – Ventersdorp Group. Age constraints are from (1) Gumsley et al., 2017[13]; (2) Trendall et al., 1990[9]; (3) Lantink et al., 2019[12]; (4) Gutzmer and Beukes, 1998[8].

Samples and methods

Samples were taken from four well-preserved drill cores stored at the National Core Library in Donkerhoek, South Africa (Figure S2). The GKF01 and GKP01 drill cores represent proximal and distal sections of the Campbellrand-Malmani carbonate platform, respectively. Correlation between these two drill cores is primarily based on sequence stratigraphy, volcanic horizons, and similar lithologies[4]. The GTF01 and GEC01 drill cores also represent respectively more proximal and distal sections for the uppermost Asbestos Hills and Koegas subgroups[7].

Iron speciation analysis was conducted via the well-established sequential extraction procedure of Poulton and Canfield (2005)[16], with pyrite Fe (Fe_{Py}) quantified gravimetrically via chromous chloride distillation[17]. Solutions from the sequential extracts were analysed via AAS, and replicate extractions gave relative standard deviations (RSDs) of <5% for all Fe phases. Total element concentrations (Fe, P, and Al) were determined on ashed samples via an HF-$HClO_4$-HNO_3 extraction, with HBO_3 used to ensure full solubilisation of Al. Solutions were analysed by ICP-OES with >98% recovery for all elements and RSDs of <5%. For organic carbon content, samples were treated with 50% vol/vol HCl prior to total organic carbon analysis using a LECO C/S analyser.

A highly reactive fraction (Fe_{HR}) is extracted from four operationally defined sedimentary phases; carbonate-associated iron (Fe_{Carb}), ferric oxides (Fe_{Ox}), mixed-valence iron oxides (principally magnetite (Fe_{Mag})), and pyrite-associated Fe (Fe_{py}). The ratio of this summed highly reactive fraction to total Fe concentration (Fe_T) is used to determine bottom-water redox conditions, whereby ratios < 0.22 are typically considered oxic, and ratios > 0.38 define anoxic conditions[18]. Intermediate values (0.22-0.38) are considered equivocal and require further investigation (see below). Further information on the redox state of the water column can be achieved via consideration of the ratio of Fe_{py} to Fe_{HR} for clearly anoxic samples (i.e., Fe_{HR}/Fe_T > 0.38), in which Fe_{py}/Fe_{HR} ratios > 0.7-0.8 identify euxinic conditions and ratios < 0.7 identify ferruginous water-column conditions. The relatively high concentrations of siderite and pyrite present in the samples suggests minimal post-depositional oxidation, as would be expected with deep drill-core samples.

Equivocal Fe_{HR}/Fe_T ratios may occur due to either rapid sedimentation (which may mask the anoxic water-column conditions and limit deposition of minerals included in the Fe_{HR} pool such that enrichments are not evident in the sediment), or due to potential conversion of highly reactive iron to Fe-rich sheet silicates, which is a common process in ferruginous settings characterised by minimal sulphate reduction (e.g., [19-21]). Fe_T/Al ratios can be used to address the latter case of diagenetic transfer of Fe_{HR} to Fe_{PRS}, since this metric is not affected by phase speciation, and ratios >0.66 are considered to provide a robust indication of anoxic water-column deposition[22]. In order to discriminate between ferruginous shale and iron formation samples, we take the classic definition of iron formation, and assign a minimum value of 20 wt% Fe to identify iron formation samples. However, we stress that this distinction does not affect any of our interpretations or conclusions.

We utilised a revised P speciation technique (originally developed by Ruttenberg, 1992[23]) for application to ancient rocks (Figure S3[24]). The sequential method targets 5 operationally defined phosphorus pools. These pools include ferric oxide-bound phosphorus (P_{Fe1} and P_{Fe2}), authigenic carbonate fluorapatite (CFA) associated P (P_{aut}), crystalline apatite-associated P (P_{cryst}), magnetite-associated P (P_{mag}), and organic-bound P (P_{org}). Here, for simplicity, we combine P_{Fe1}, P_{Fe2}, and P_{mag} to give the total P pool associated with Fe-oxide minerals (P_{Fe}). Phosphorus concentrations were generally determined spectrophotometrically on a Spectonic GENESYS™ 6 at 880 nm, using the molybdate-blue method[25]. However, the chemicals in the P_{Fe} (CDB and CDA; see Figure S3) and P_{mag} (ammonium oxalate) solutions interfere with colour development, and hence these solutions were analysed with ICP-OES (for specific details of ICP-OES configuration see Thompson et al., 2019[24]).

On average, the summed sequential P extractions recovered 94% of the total P measured by bulk digest. Replicate analyses gave an RSD of ~10% for P_{aut} and P_{cryst} in addition to P_{mag} and P_{org} both providing a RSD of <13%. P_{Fe} was at very low concentration in our samples (close to the limit of detection), but the RSD for such analyses is generally ~3% when P_{Fe} is present above trace concentrations[24], and the very low concentrations of P_{Fe} in our samples do not affect the interpretation of our P speciation data (see the main text). For the calculation of the average C_{org}:P_{org} ratios (see the

main text) we only utilised P_{org} data for samples, which were above the limit of quantification (9.90 ppm).

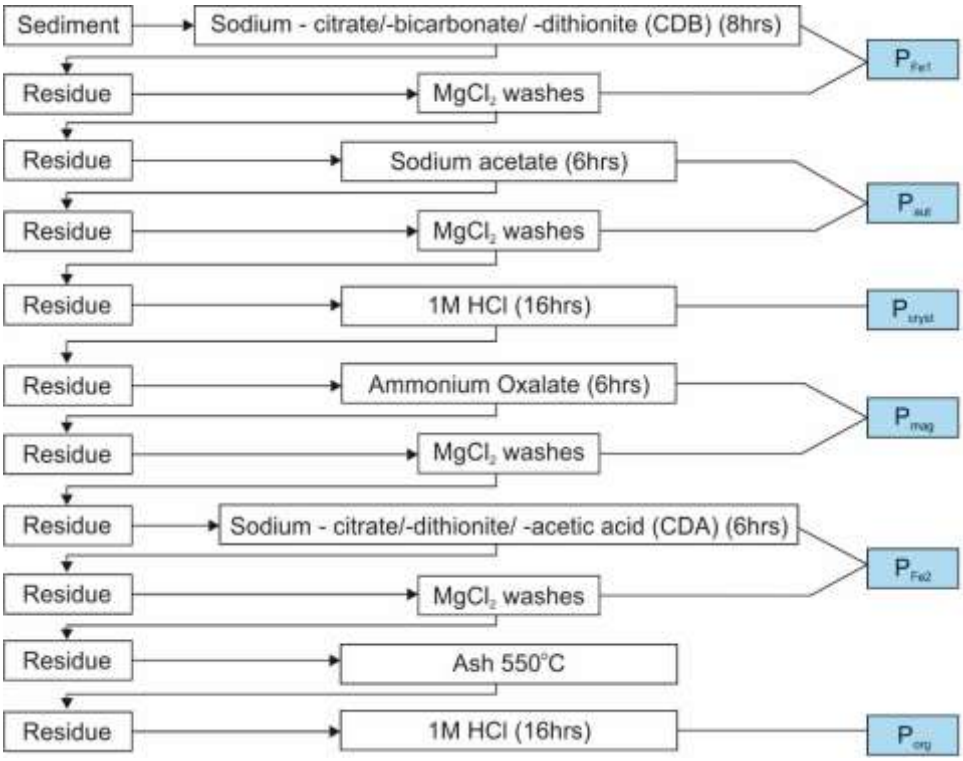

Figure S3.Sequential extraction procedure for phosphorus (Thompson et al., 2019).

Biogeochemical modelling

We utilise a modified 5 box ocean-atmosphere biogeochemical model for C-O-P cycling over Earth history[26] to examine the response to altering P weathering and varying C_{org}:P_{org} ratios of buried material. The model was originally devised by Slomp and Van Cappellen (2007)[27], and later modified by Tsandev et al. (2008)[28], Tsandev and Slomp (2009)[29], and Alcott et al. (2019)[26]. The full model equations are presented in Alcott et al. (2019)[26], and are briefly summarised here. The 4 ocean boxes represent regions of the proximal and distal coastal shelf along with the surface and deep oceans. These marine boxes consider organic carbon, organic phosphorus, soluble phosphorus, and oxygen. A fifth box represents the atmosphere, where only oxygen is considered. The model includes productivity, remineralization, and burial of organic carbon, and 3 separate phosphorus phases. The

189 redox-dependent P burial phases considered in the model consist of P_{org}, iron-oxide bound P_{Fe}, and
190 authigenic P_{aut}.

191 In this paper we modify the original model of Alcott et al. (2019)[26] in order to accommodate the
192 results from this dataset: we considered values for the maximum C_{org}:P_{org} burial ratio under anoxic
193 conditions to be between 100 and 10,000. We also varied the input of P from continental weathering
194 from 1 to 100% of the present-day flux. We plot steady states with respect to both P input and C:P
195 ratio for a fixed amount of oxygen consumption via reductant input following the values used in
196 Alcott et al. (2019)[26] for ~2.4 Ga (1.5×10^{13} mol yr^{-1}). All model equations are listed below and are
197 fully summarised in Alcott et al. (2019), to which we direct the reader for further discussion of the
198 model. The model schematic is shown in Figure S4.

199 We acknowledge the limitations and assumptions made via the use of this model and its approach.
200 First, we simulate elevated C:P ratios in organic matter by defining a maximum ratio that may occur
201 under anoxic conditions, as opposed to a fully realised iron and sulfur cycle model. The Earth's
202 surface redox budget has been described and quantified previously[30]. When compared to the oxygen
203 sink fluxes considered in the model (reduced gases and oxidative weathering), the modern-day burial
204 flux of gypsum and iron oxides is around two orders of magnitude smaller than the fluxes we have
205 included. This discrepancy would become more apparent under the sulfate limited and anoxic
206 conditions of the Archean.

207 With respect to sources of oxygen, pyrite burial is only a factor of two smaller than organic carbon
208 burial at present day. However, during the Archean, ocean sulfate concentrations were significantly
209 lower than present day[31]. Based on the less prevalent sulfur cycle and these quantitative estimates,
210 feedbacks related to the iron and sulfur cycles would not diminish our overall conclusions, and indeed
211 the impact of these cycles is included in the range of C_{org}:P_{org} ratios we utilise in the model. In
212 addition, we do not consider potential variability in the concentrations of other seawater ions, such as
213 calcium, which have been suggested to impact sedimentary P retention through formation of
214 carbonate-fluorapatite[32]. However, while the concentration of seawater Ca^{2+} is not well-constrained
215 for this time period, the impact of modest variability in Ca^{2+} across the interval of study would be

overwhelmed by the huge degree of recycling that is clearly evident from consideration of the measured C_{org}/P_{org} and C_{org}/P_{reac} ratios. Indeed, P associated with carbonate-fluorapatite is the dominant phase extracted as part of the P_{aut} pool[33], and we determined appreciable concentrations of this phase relative to P_{org}, suggesting that this was not a major limitation on P retention in the sediment.

A more detailed modelling approach, for example taking into account variability in C_{org}:P_{org} ratios with respect to water depth[34], may allow for a more high resolution modelling output. However, the variability in C_{org}:P_{org} ratios found via our phosphorus speciation analyses is two orders of magnitude larger than that which may occur as a consequence of changes in water depth[34], and thus our conclusions would be unaffected by this consideration.

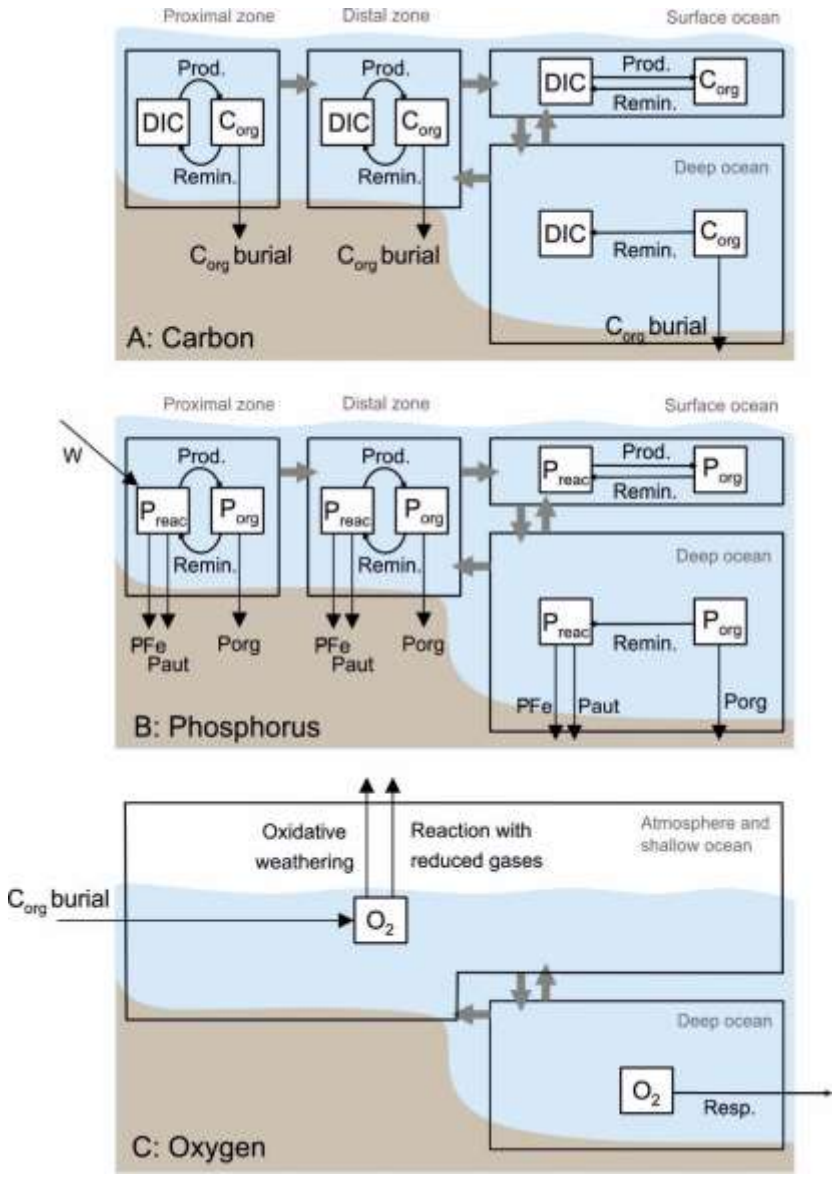

227

228 *Figure S4. Ocean and atmosphere box model. Clear boxes show hydrospheric reservoirs and grey*
229 *arrows denote mixing between them. White boxes show chemical reservoirs and black arrows denote*
230 *biogeochemical fluxes. (A) Carbon cycle: C exists as dissolved inorganic carbon (DIC) or organic*
231 *carbon (C_{org}). (B) Phosphorus cycle: P exists as soluble reactive phosphorus (P_{reac}) and particulate*
232 *organic phosphorus (P_{org}). (C) Oxygen cycle. Single oxygen reservoir encompasses all ocean boxes*
233 *that exchange with the atmosphere. See text for full description, and methods and SI for equations.*

234

235

236

237

238 **Table S1: Present day reservoirs with the corresponding flux equations.** Present day steady-state
239 values and fluxes are presented below.

Reservoir	Eq No.	Label	Initial Size (moles)	Differential Equation	Source
Proximal Water	1	W_P	$36x10^{12}$	$River_W - circ_{PD}$	[1]
Distal Water	2	W_D	$3600x10^{12}$	$circ_{PD} + circ_{DPD} - circ_{DS}$	[1]
Surface Water	3	W_S	$4{,}983x10^{13}$	$circ_{DPS} + circ_{DS} - circ_{SDP} - Evap$	[1]
Deep Ocean Water	4	W_{DP}	$1.3x10^{18}$	$circ_{SDP} - circ_{DPS} - circ_{DPD}$	[1]
Proximal Carbon	5	C_P	$4.5x10^{12}$	$PP_P - POCmin_P - POCbur_P - xp_{PD}$	[1]
Distal Carbon	6	C_D	$243x10^{12}$	$xp_{PD} + PP_D - POCbur_D - POCmin_D - xp_{DS}$	[1]
Surface Carbon	7	C_S	$3{,}816x10^{12}$	$xp_{DS} + PP_S - POCmin_S - xp_{SDP}$	[1]
Deep Ocean Carbon	8	C_{DP}	$5.6x10^{16}$	$xp_{SD} - RespPOC - POCbur_{DP}$	[1]
Proximal Oxygen	9	O_P	$4.5x10^{12}$	$O_{P_0} \cdot \boldsymbol{O_A}$	[1]
Distal Oxygen	10	O_D	$243x10^{12}$	$O_{D_0} \cdot \boldsymbol{O_A}$	[1]
Surface Oxygen	11	O_S	$1.615x10^{16}$	$O_{S_O} \cdot \boldsymbol{O_A}$	[1]
Deep Ocean Oxygen	12	O_{DP}	$2.21x10^{17}$	$O_{SDP} - OResp - O_{DPS} - O_{DPD}$	[1]
Atmosphere Oxygen	13	O_A	$3.7x10^{19}$	$POCburT - AtmosW - genred$	[2]
Proximal SRP	14	P_P	$9.7x10^{9}$	$W_P - PPP_P + POPmin_P - PFe_P - Pauth_P - SRP_{PD}$	[1]
Distal SRP	15	P_D	$5x10^{12}$	$SRP_{PD} - PPP_D + POPmin_D - PFe_D - Pauth_D - SRP_{DS} + SRP_{DPD}$	[1]
Surface SRP	16	P_S	$47x10^{12}$	$SRP_{DS} - PPP_S + POPmin_S - SRP_{SDP} + SRP_{DPS}$	[1]
Deep Ocean SRP	17	P_{DP}	$2{,}790x10^{12}$	$SRP_{SDP} + POPmin_{DP} - PFe_P - Pauth_{DP} - SRP_{DPS} - SRP_{DPD}$	[1]
Proximal POP	18	OP_P	$4.3x10^{10}$	$PPP_P - POPmin_P - POPbur_P - POP_{PD}$	[1]
Distal POP	19	OP_D	$2.3x10^{12}$	$POP_{PD} + PPP_D - POPmin_D - POPbur_D - POP_{DS}$	[1]
Surface POP	20	OP_S	$36x10^{12}$	$POP_{DS} + PPP_S - POPmin_S - POP_{SDP}$	[1]
Deep Ocean POP	21	OP_{DP}	$530x10^{12}$	$POP_{SDP} - POPmin_{DP} - POPbur_{DP}$	[1]

240

241 **Table S2: Present day flux values and corresponding equations.**

Flux	Eq No.	Label	Initial flux (moles/yr)	Equation	Source
River input	22	$River_W$	$37x10^{12}$	$constant$	[1]

Proximal-Distal water	23	$circ_{PD}$	37x10^{12}	$constant$	[1]
Low latitude upwelling water	24	$circ_{DPD}$	3.78x10^{14}	$kDpD \cdot W_{DP}$	[1]
Distal- Surface ocean water	25	$circ_{DS}$	4.15x10^{14}	$circ_{PD} + circ_{DPD}$	[1]
High latitude upwelling water	26	$circ_{DPS}$	3.78x10^{15}	$kDpS \cdot W_{DP}$	[1]
High latitude downwelling water	27	$circ_{SDP}$	4.158x10^{15}	$kSDp \cdot W_S$	[1]
Evaporation of surface water	28	$Evap$	37x10^{12}	$River_W$	[1]
Proximal Primary Production OC	29	PP_P	3.975x10^{13}	$kPP_P \cdot \boldsymbol{P_P} \cdot RedCP$	[1]
Proximal OC mineralisation	30	$POCmin_P$	3.277x10^{13}	$kcmin_P \cdot \boldsymbol{C_P}$	[1]
Proximal OC burial	31	$POCbur_P$	2.3x10^{12}	$kcbur_P \cdot PP_P$	[1]
Proximal-Distal export prod.	32	xp_{PD}	4.685x10^{12}	$POP_{PD} \cdot RedCP$	[1]
Distal Primary Production OC	33	PP_D	5.6x10^{14}	$kPP_D \cdot \boldsymbol{P_D} \cdot RedCP$	[1]
Distal OC burial	34	$POCbur_D$	1.7x10^{12}	$kcbur_D \cdot (xp_{PD} + PP_D)$	[1]
Distal OC mineralisation	35	$POCmin_D$	5.349x10^{14}	$kcmin_D \cdot \boldsymbol{C_D}$	[1]
Distal-Surface export prod.	36	xp_{DS}	2.811x10^{13}	$POP_{DS} \cdot RedCP$	[1]
Surface Ocean Primary Production	37	PP_S	3.869x10^{15}	$kPP_S \cdot \boldsymbol{P_S} \cdot RedCP$	[1]*
Surface OC mineralisation	38	$POCmin_S$	3.404x10^{15}	$kcmin_S \cdot \boldsymbol{C_S}$	[1]*
Surface-Deep export prod.	39	xp_{SDP}	4.931x10^{14}	$kxp_{SDP} \cdot (xp_{DS} + PP_S)$	[1]*
OC Respiration	40	$RespPOC$	4.921x10^{14}	$kResp \cdot \boldsymbol{C_{DP}}$	[1]*
Deep Ocean OC burial	41	$POCbur_{DP}$	1 x10^{12}	$POPburd_{DP} \cdot \frac{(CP_{anoxic} \cdot CP_{oxic})}{([\boldsymbol{O_{DP}}] \cdot CP_{anoxic}) + ((1 - [\boldsymbol{O_{DP}}]) \cdot CP_{oxic})}$	[1]*
Surface-Deep oxygen downwelling	42	O_{SDP}	1.347x10^{15}	$circ_{SDP} \cdot [O_s]$	[1]*
Oxygen Respiration	43	$OResp$	6.403x10^{14}	$kResp \cdot (\frac{\boldsymbol{C_{DP}}}{redCO}) \cdot (\frac{O_{DP}}{(kmO_2 + O_{DP})})$	[1]*
Deep-Surface oxygen upwelling	44	O_{DPS}	6.426x10^{14}	$circ_{DPS} \cdot [O_{DP}]$	[1]
Deep-Distal oxygen upwelling	45	O_{DPD}	6.426x10^{13}	$circ_{DPD} \cdot [O_{DP}]$	[1]
Total OC burial	46	$POCburT$	5x10^{12}	$POCbur_P + POCbur_D + POCbur_{DP}$	[4]
Oxidative Weathering	47	$AtmosW$	5x10^{12}	$kAtmosW \cdot (\sqrt{\boldsymbol{O_A}})$	[4]
Oxygen consumption via reduced gases	48	$genred$	0	Varied in ms figs 3-5 fixed in figs S1, S4 panels g-i	[4]
Riverine P input	49	W_P	9x10^{10}	Fixed in ms figs 3-5, varied in figs S1, S4 panels g-i.	[1]
Proximal Primary Production (P)	50	PPP_P	3.75x10^{11}	$\frac{PP_P}{RedCP}$	[1]

Proximal POP mineralisation	51	$POPmin_P$	3.216×10^{11}	$\boldsymbol{OP_P} \cdot kpmin_P$	[4]
Proximal Iron bound P burial	52	PFe_P	8.973×10^{9}	$kFeP_P \cdot P_P$	[4]
Proximal Authigenic P burial	53	$Pauth_P$	1.768×10^{10}	$kpmin_P \cdot OP_P \cdot kCaP_P$	[4]
Proximal-Distal SRP transport	54	SRP_{PD}	9.969×10^{9}	$circ_{PD} \cdot [P_P]$	[4]
Distal Primary Production (P)	55	PPP_D	5.283×10^{12}	$\frac{PP_D}{RedCP}$	[1]
Distal POP mineralisation	56	$POPmin_D$	5.055×10^{12}	$\boldsymbol{OP_P} \cdot kpmin_D$	[4]
Distal Iron bound P burial	57	PFe_D	6.762×10^{9}	$kFeP_D \cdot P_D \cdot (1 - fanoxic_{dist})$	[3]
Distal Authigenic P burial	58	$Pauth_D$	1.032×10^{10}	$kCaP_D \cdot \boldsymbol{O_D} \cdot (1 - fanoxic_{dist})$	[3]
Distal-Surface SRP transport	59	SRP_{DS}	5.764×10^{11}	$circ_{DS} \cdot [P_D]$	[1]
Deep-Distal SRP transport	60	SRP_{DPD}	8.113×10^{11}	$circ_{DPD} \cdot [P_{DP}]$	[1]
Surface Ocean Primary Production (P)	61	PPP_S	3.650×10^{13}	$\frac{PP_S}{RedCP}$	[1]*
Surface POP mineralisation	62	$POPmin_S$	3.173×10^{13}	$OP_S \cdot kpmin_S$	[4]
Surface-Deep SRP transport	63	SRP_{SDP}	3.922×10^{12}	$circ_{SDP} \cdot [P_S]$	[1]
Deep-Surface SRP transport	64	SRP_{DPS}	8.113×10^{12}	$circ_{DPS} \cdot [P_{DP}]$	[1]
Deep POP mineralisation	65	$POPmin_{DP}$	5.028×10^{12}	$OP_{DP} \cdot kpmin_{DP}$	[4]
Deep Iron bound P burial	66	PFe_{DP}	6.75×10^{9}	$kFeP_{DP} \cdot [\boldsymbol{O_{DP}}]$	[3]
Deep Authigenic P burial	67	$Pauth_{DP}$	1.953×10^{10}	$kCaP_{DP} \cdot POPmin_{DP} \cdot (0.75 + (0.25 \cdot [\boldsymbol{O_{DP}}]))$	[3]
C:P ratio for respective box	68	$CPratio$	250 (oxic) 1100 (anoxic)	$\frac{1}{\left(\frac{1 - fanoxic_x}{CP_{oxic}}\right) + \left(\frac{fanoxic_x}{CP_{anoxic}}\right)}$	[1]
Proximal POP burial	69	$POPbur_P$	9.182×10^{9}	$kcbur_P \cdot \frac{PP_P}{CPratio_{proximal}}$	[4]
Proximal-Distal POP transport	70	POP_{PD}	4.419×10^{10}	$circ_{PD} \cdot [OP_P]$	[4]
Distal POP burial	71	$POPbur_D$	6.800×10^{9}	$kPOPbur_d \cdot \frac{PP_D + xp_{PD}}{CPratio_{distal}}$	[4]
Distal-Surface POP transport	72	POP_{DS}	2.651×10^{11}	$circ_{DS} \cdot [OP_D]$	[4]
Surface-Deep POP transport	73	POP_{SDP}	5.032×10^{12}	$kPOP_{SDP} \cdot (\frac{PP_S + xp_{DS}}{RedCP})$	[4]
Deep POP burial	74	$POPburd_{DP}$	4×10^{9}	$kPOPbur_{DP} \cdot \left(\frac{xp_{SDP}}{CP_{oxic}}\right) \cdot (0.75 + (0.25 * [\boldsymbol{O_{DP}}]))$	[3]

242

243 OC-Organic Carbon, SRP-Soluble Reactive Phosphorous, POP-Particulate Organic Phosphorus

244 *Flux equation is the same as citation, however present day value was altered by Alcott et al. (2019)

[1] – Slomp and Van Cappellen (2007)[27]

[2] – Bergman et al. (2004)[35]

[3] – Tsandev and Slomp (2009)[29]

[4] – Alcott et al. (2019)[26]

Table S3: Parameters and constants.

Parameter/ Constant	Constant	Value	Reference
Coastal Upwelling	$kDpD$	2.908×10^{-4}	Slomp and Van Cappellen, 2007
Open Ocean Upwelling	$kDpS$	0.0029	Slomp and Van Cappellen, 2007
Open Ocean Downwelling	$kSDp$	0.0834	Slomp and Van Cappellen, 2007
Proximal shelf primary production	kPP_P	3.75×10^{11}	Slomp and Van Cappellen, 2007
Proximal organic carbon remineralisation	$kcmin_P$	3.277×10^{13}	This work
Proximal organic carbon burial	$kcbur_P$	0.0579	Slomp and Van Cappellen, 2007
Distal shelf primary production	kPP_D	5.283×10^{12}	Slomp and Van Cappellen, 2007
Distal organic carbon burial	$kcbur_D$	0.003	Slomp and Van Cappellen, 2007
Distal organic carbon remineralisation	$kcmin_D$	5.349×10^{14}	This work
Surface ocean primary production	kPP_S	3.650×10^{13}	Slomp and Van Cappellen, 2007
Surface organic carbon remineralisation	$kcmin_S$	3.404×10^{15}	This work
Surface to Deep Ocean export production	kxp_{SDP}	0.1265	Slomp and Van Cappellen, 2007
Deep Ocean Respiration	$kResp$	4.921×10^{14}	Slomp and Van Cappellen, 2007
Deep ocean organic carbon burial	$kcbur_{DP}$	0.0019	Slomp and Van Cappellen, 2007
Monod constant for respiration	kmO_2	1×10^{-4}	Slomp and Van Cappellen, 2007
Oxidative Weathering	$kAtmosW$	5×10^{12}	Alcott et al., 2019
Carbon – Phosphorus Redfield ratio	$RedCP$	106	Slomp and Van Cappellen, 2007
Proximal Iron bound P burial	$kFeP_P$	0.925	Alcott et al., 2019
Proximal Authigenic P burial	$kCaP_P$	1.279×10^{-12}	Alcott et al., 2019
Distal Iron bound P burial	$kFeP_D$	0.0014	Alcott et al., 2019
Distal Authigenic P burial	$kCaP_D$	1.035×10^{10}	Alcott et al., 2019
Deep ocean Iron bound P burial	$kFeP_{DP}$	6.75×10^{9}	Alcott et al., 2019
Deep ocean Authigenic P burial	$kCaP_{DP}$	0.0039	Alcott et al., 2019
Distal Organic P burial	$kPOPbur_D$	0.003	Alcott et al., 2019
Surface to Deep Organic Phosphorus Export Production	$kPOP_{SDP}$	0.1369	Alcott et al., 2019
Deep Ocean Organic P burial	$kPOPbur_{DP}$	0.002	Alcott et al., 2019

P Speciation

Consideration of possible late-stage diagenetic P phase alteration is required when applying P speciation to ancient sedimentary rocks[24,36]. The main issue that might affect interpretation of P speciation data (which utilises two P pools: P_{org} and P_{reac}; see the main text) is the potential for recrystallization of carbonate fluorapatite (P_{aut}) to more crystalline apatite (P_{cryst}). Although P_{cryst} does constitute a significant proportion in some of our samples (~66% on average for the GKF01 and GKP01 drill cores), we note that there is no correlation between P_{aut} and P_{cryst} (Figure S5) and particularly high P_{cryst}/Al ratios only tend to occur at euxinic to ferruginous transitions, as shown by excursions in the P_{cryst}/Al ratio (Figure S6). Therefore, while a portion of the authigenic phase may have been recrystallized, it does not detract from our overall interpretation and would only support our hypothesis of greater fixation of P within the sediment during ferruginous conditions, as more P would be included within our P_{reac} phase (shifting a minor proportion of the ferruginous data in Figure 2 of the main text, to below or, at least, more towards the Redfield Ratio of 106:1). We can also demonstrate recycling of P from the sediment based on the ratio of C_{org}:P_{total} (P_{total}; total P by bulk digest) (Figure S7). The GKF01 and GKP01 drill cores demonstrate P recycling based on C_{org}:P_{reac} and C_{org}:P_{org} ratios (see the main text), but they even have several samples that plot above the Redfield Ratio with the inclusion of all the P phases. By contrast, samples of the Koegas Subgroup from the GTF01 and GEC01 drill cores exclusively plot below the Redfield ratio with the inclusion of the additional P phases (primarily P_{cryst}). This overall trend further supports recycling of P from the sediment under sulfidic porewater/euxinic water-column conditions regardless of the extent of conversion of P_{aut} to P_{cryst}.

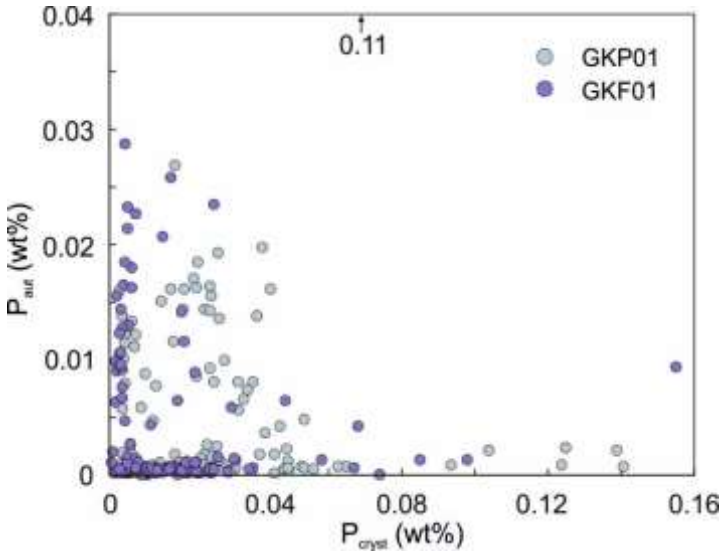

Figure S5. P_{cryst} vs. P_{aut} plot for all samples analyzed for P speciation from the GKP01 and GKF01 drill cores.

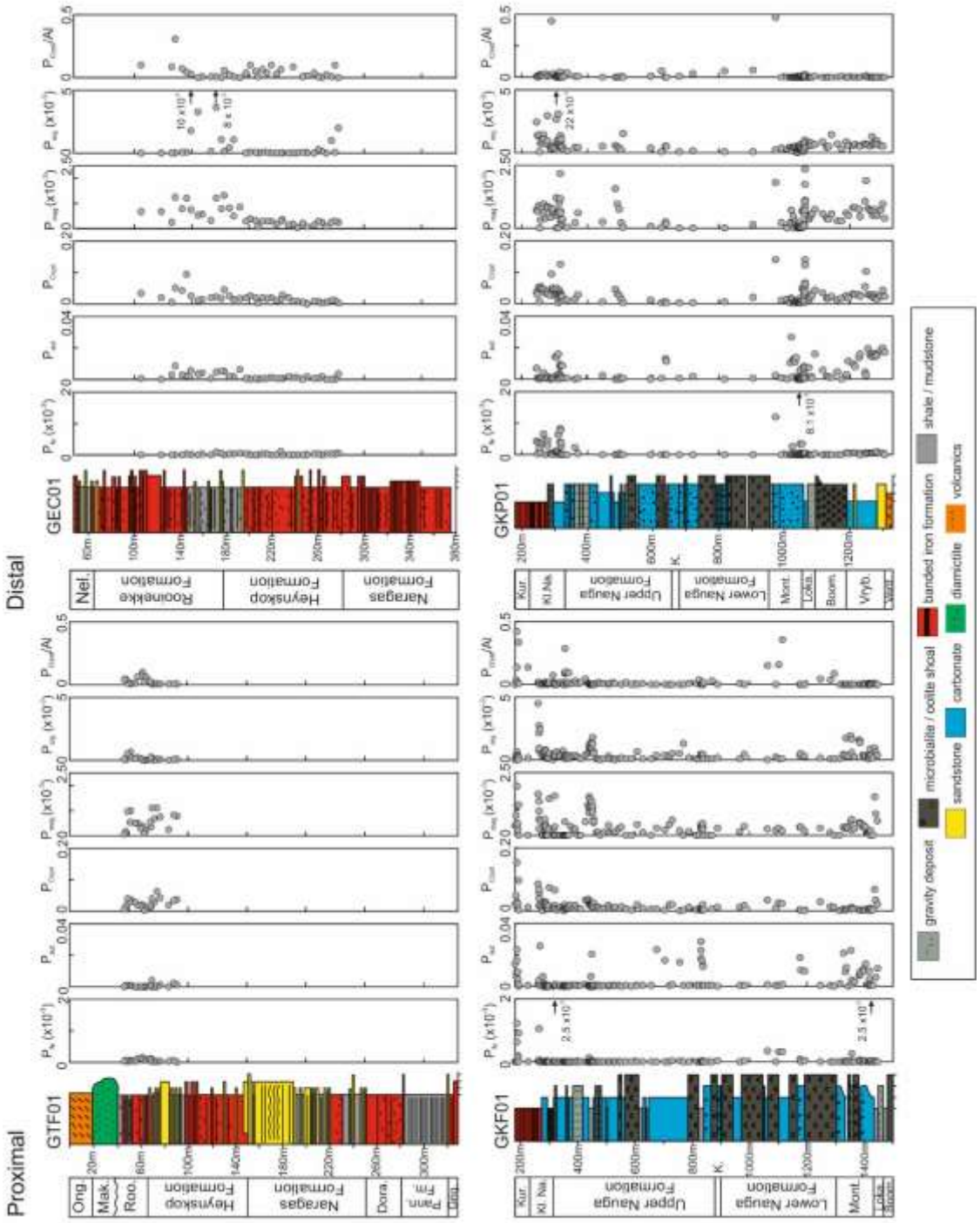

286 *Figure S6. P speciation data for drill-core samples (wt%). (A) Proximal GTF01 drill core. (B) Distal*
287 *GEC01 drill core. (C) Proximal GKF01 drill core. (D) Distal GKP01 drill core.* P_{Fe} *(Fe-associated*
288 *P),* P_{aut} *(authigenic P),* P_{Cryst} *(highly crystalline P),* P_{mag} *(magnetite-associated P) and* P_{org} *(organic-*
289 *associated P). Abbreviations for formations: Ong. – Ongeluk Formation; Mak. – Makganyene*
290 *Formation; Roo. – Rooinekke Formation; Dora. – Doredale Formation; Pann. – Pannetjie*
291 *Formation; Griq. – Griquatown Iron Formation; Nel. – Nelani Formation; Dwyka. – Dwyka*
292 *Formation; Kur. – Kuruman Iron Formation; Kl. Na. – Klein Naute Formation; K. – Kamden*
293 *Member; Mont. – Monteville Formation; Loka. – Lokamonna Formation; Boom. – Boompaas*
294 *Formation; Vryb. – Vryburg Formation; Vent. – Ventersdorp Group.*

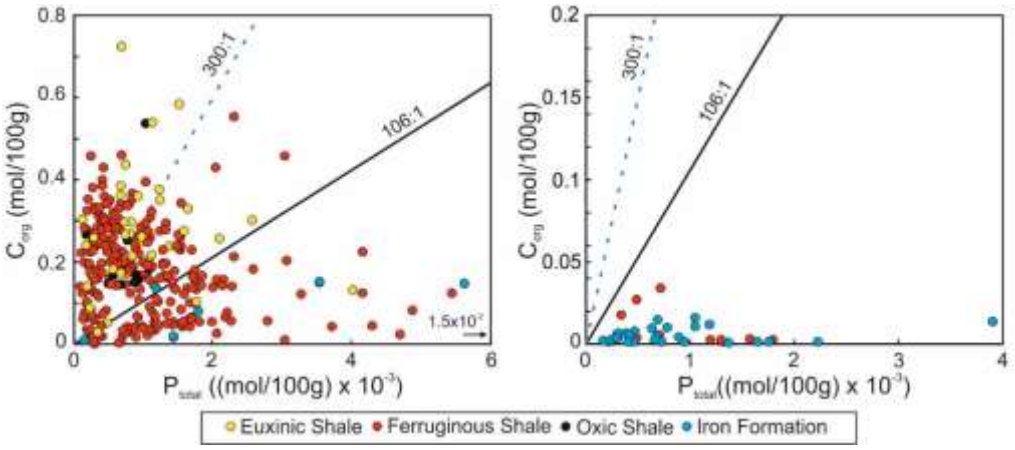

Figure S7. Relationship between organic carbon and total phosphorus. (A) C_{org}/P_{total} for the Ghaap Group drill cores (GKF01 and GKP01); (B) C_{org}/P_{total} for the Koegas Subgroup drill cores (GTF01 and GEC01). Solid line represents the Redfield Ratio (106:1), and the dashed line represents the inferred C_{org}/P_{org} ratio for the early Precambrian sediments deposited under highly oligotrophic, P-limited conditions (Reinhard et al., 2017).

Distinguishing between sulphidic porewaters and euxinic water-column conditions

As discussed in the main text, two horizons in the succession have elevated Fe_{HR}/Fe_T and Fe_{py}/Fe_{HR} ratios that might suggest euxinic water-column conditions. However, such a signal may also be generated during intense sulphide production in pore waters close to the sediment-water interface beneath a ferruginous water column. To address this possibility we consider the morphology of pyrite in the two horizons. In the case of the older Monteville Formation samples, reflected light microscopy shows abundant evidence for wavy layers, rip up clasts and nodules, and poorly disseminated coarser-grained euhedral pyrite (Figure S8). These features are not typical of textures commonly found when iron sulphide formation is dominantly instigated in a euxinic water column, where instead, fine-grained dispersed pyrite tends to dominate[37]. We thus suggest that the high Fe_{HR}/Fe_T and Fe_{py}/Fe_{HR} ratios evident for these samples most likely reflect intense diagenetic pyrite formation close to the sediment-water interface beneath a dominantly ferruginous water column. By contrast, pyrite in the younger Klein Naute Formation consists of fine, well-disseminated pyrite, with only occasional larger euhedral grains likely formed during diagenesis. Indeed, the pyrite morphology of these samples has been suggested to dominantly comprise relic framboids[38], and their small size and limited size range is more consistent with morphologies found in sediments deposited under a euxinic water column[32]. In addition, published trace metal systematics for the Klein Naute Formation also suggest intervals of

euxinic deposition[39]. Thus, when considered in combination, the Fe speciation, trace element and pyrite morphological characteristics are consistent with a conventional interpretation of deposition from a euxinic water column.

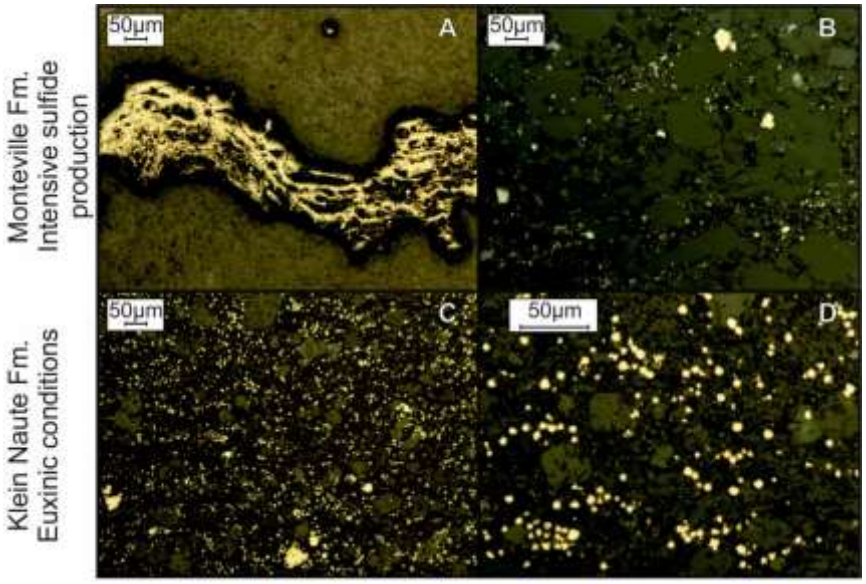

Figure S8. Images of pyrite morphologies within the two stratigraphic intervals with elevated Fe_{py}/Fe_{HR} ratios. A, B - layered and nodular pyrite of the Monteville Formation. C, D - disseminated and euhedral pyrite of the Klein Naute Formation.

Model results with elevated weathering fluxes

The phosphorus input flux to the ocean at 2.5 Ga has been estimated based on weathering kinetics and continental emergence times[40]. The central estimates show negligible weathering in the Early Archean, rising to a flux within ~0.4 to ~1.2 times the present day, but with a maximum error up to ~3 times present day. In the manuscript we test the central estimates of this flux in a biogeochemical model, and here we extend the estimates up to 3x present (Figure S9). It is possible to see that when no P recycling is considered (maximum primary C_{org}:P_{org} of ~300)[41], the absolute maximum (and unlikely) weathering fluxes are required in order to provide oxygenation on the scale of the GOE, supporting our interpretation of phosphorus recycling facilitating planetary oxygenation.

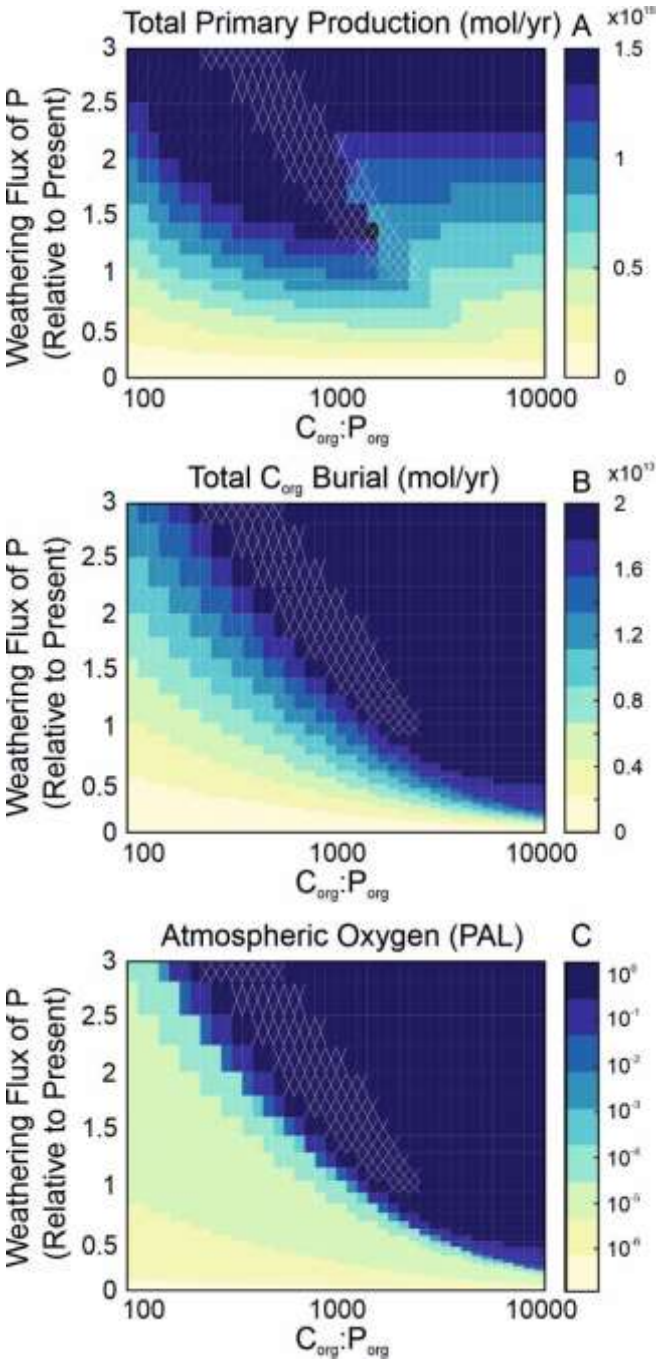

Figure S9. Steady-state model solutions for a fixed reduced gas flux of 15 x 10^{12} (O_2 equivalents yr^{-1}). (A) Total primary production (mol C yr^{-1}). (B) Total organic carbon burial (mol C yr^{-1}). (C) Atmospheric oxygen concentration relative to Present Atmospheric Level (PAL). Model runs that produce non-steady state results have been interpolated with respect to neighbouring results and are indicated by crosses.

Model results with a lower reduced gas flux

Oxidation events are induced in the model by increasing the availability of phosphorus, either through increased phosphorus input via weathering, or recycling of phosphorus. The timing of oxygenation is, however, regulated by the input of reduced gases into the model atmosphere. It is important to emphasize that the phosphorus speciation data presented here demonstrate over an order of magnitude change in P recycling, while the degree of change in the mantle flux of reductants is very unlikely[42]. Figure S10 shows a lower reduced gas flux than those shown previously, demonstrating the control this flux has on the bounds of oxygenation. A lesser flux of organic carbon burial is required in order to lead to a Great Oxidation Event, but an increase is still required, relative to pre-oxidation conditions.

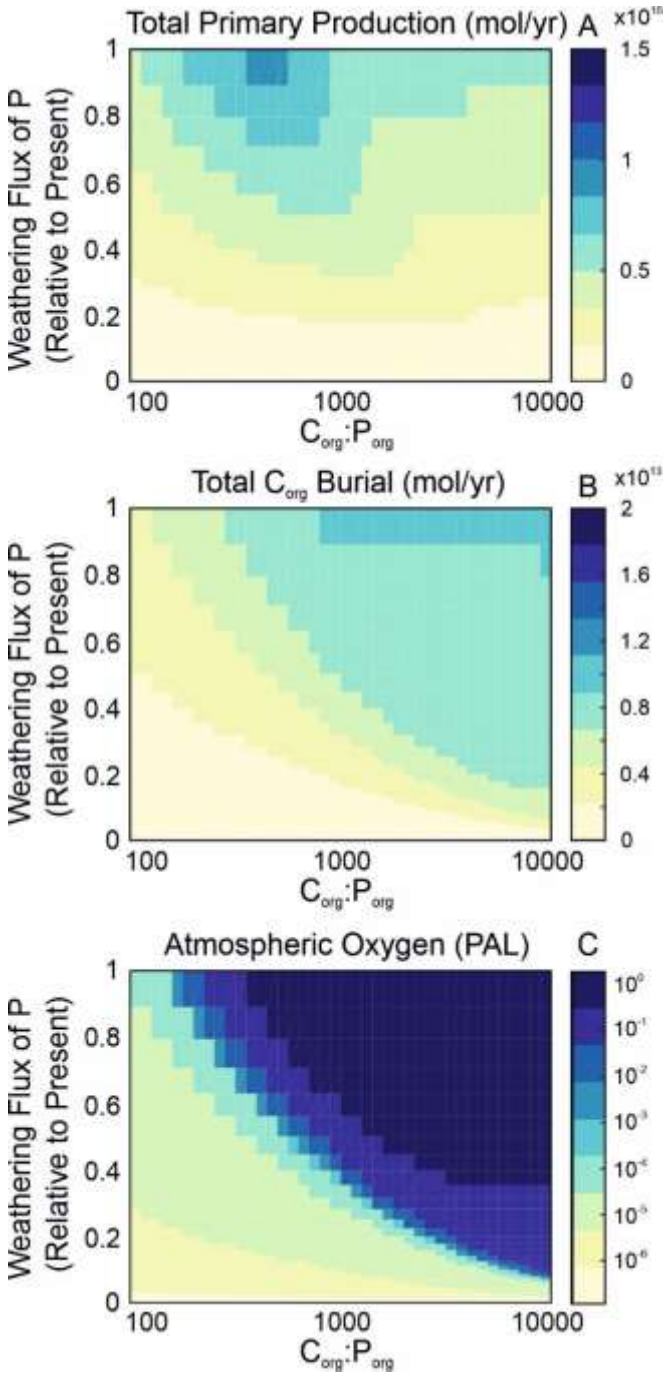

Figure S10. Steady-state model solutions for a fixed reduced gas flux of 5 x 10^{12} (O_2 equivalents yr^{-1}). (A) Total primary production (mol C yr^{-1}). (B) Total organic carbon burial (mol C yr^{-1}). (C) Atmospheric oxygen concentration relative to Present Atmospheric Level (PAL). Model runs that produce non-steady state results have been interpolated with respect to neighbouring results and are indicated by crosses.

References

1 James, D. E. & Fouch, M. J. Formation and evolution of Archaean cratons: Insights from southern Africa. *Geological Society of London Special Publications* **199**, 1-26 (2002).

2 Moore, J. M., Tsikos, H. & Polteau, S. Deconstructing the Transvaal Supergroup, South Africa: implications for Palaeoproterozoic palaeoclimate models. *Journal of African Earth Sciences* **33** (2001).

3 Kendall, B., Brenneck, G. A., Weyer, S. & Anbar, A. D. Uranium isotope fractionation suggests oxidative uranium mobilization at 2.50 Ga. *Chemical Geology* **362**, 105-114 (2013).

4 Schröder, S. Stratigraphic and geochemical framework of the Agouron drill cores, Transvaal Supergroup (Neoarchean-Paleoproterozoic, South Africa). *South African Journal of Geology* **109**, 23-54, doi:10.2113/gssajg.109.1-2.23 (2006).

5 Altermann, W. & Nelson, D. R. Sedimentation rates, basin analysis and regional correlations of three Neoarchaean and Palaeoproterozoic sub-basins of the Kaapvaal craton as inferred from precise U-Pb zircon ages from volcaniclastic sediments. *Sedimentary Geology* **120**, 225-256 (1998).

6 Sumner, D. Y. & Grotzinger, J. P. Implications for Neoarchaeanocean chemistry from primary carbonate mineralogy of the Campbellrand-Malmani Platform, South Africa. *Sedimentology* **51**, 1-27 (2004).

7 Schröder, S., Bedorf, D., Beukes, N. J. & Gutzmer, J. From BIF to red beds: Sedimentology and sequence stratigraphy of the Paleoproterozoic Koegas Subgroup (South Africa). *Sedimentary Geology* **236**, 25-44, doi:10.1016/j.sedgeo.2010.11.007 (2011).

8 Gutzmer, J. & Beukes, N. J. High-grade manganese res in the Kalahari Manganese Field: Characterisation and dating of ore-forming events. *Final Technical Report* (1998).

9 Trendall, A. F. *et al.* Precise zircon U-Pb chronological comparison of the volcano-sedimentary sequences of the Kaapvaal and Pilbara cratons between about 3.1 and 2.4 Ga. *Third International Archaean Symposium*, 81-83 (1990).

10 Pickard, A. L. SHRIMP U-Pb zircon ages for the Palaeoproterozoic Kuruman Iron Formation, Northern Cape Province, South Africa: evidence for simultaneous BIF deposition on Kaapvaal and Pilbara Cratons. *Precambrian Research* **125**, 275-315 (2003).

11 Beukes, N. J. Sedimentology of the Kuruman and Griquatown Iron-formations, Transvaal Supergroup, Griqualand West, South Africa *Precambrian Research* **24**, 47-84 (1984).

12 Lantink, M. L., Davies, J. H. F. L., Mason, P. R. D., Schaltegger, U. & Hilfen, F. J. Climate control on banded iron formations linked to orbital eccentricity. *Nature Geoscience* **12**, 369-374 (2019).

13 Gumsley, A. P. *et al.* Timing and tempo of the Great Oxidation Event. *PNAS* **114**, 1811-1816 (2017).

14 Beukes, N. J. *Die karbonaatgesteentes en ysterformasies van die Ghaap-Groep van die Transvaal-Supergroep in Noord-Kaapland*, Rand Afrikaans University, (1978).

15 Kurzweil, F., Wille, M., Gantert, N., Beukes, N. J. & Schoenberg, R. Manganese oxide shuttling in pre-GOE oceans – evidence from molybdenum and iron isotopes. *Earth and Planetary Science Letters* **452**, 69-78, doi:10.1016/j.epsl.2016.07.013 (2016).

16 Poulton, S. W. & Canfield, D. E. Development of a sequential extraction procedure for iron: implications for iron partitioning in continentally derived particulates. *Chemical Geology* **214**, 209-221, doi:10.1016/j.chemgeo.2004.09.003 (2005).

17 Canfield, D. E., Raiswell, R., Westrich, J. T., Reaves, C. M. & Berner, R. A. The use of chromium reduction in the analysis of reduced inorganic sulfur in sediments and shales. *Chemical Geology* **54**, 149-155 (1986).

18 Poulton, S. W. & Canfield, D. E. Ferruginous Conditions: A Dominant Feature of the Ocean through Earth's History. *Elements* **7**, 107-112, doi:10.2113/gselements.7.2.107 (2011).

19 Poulton, S. W., Fralick, P. W. & Canfield, D. E. Spatial variability in oceanic redox structure 1.8 billion years ago. *Nature Geoscience* **3**, 486-490, doi:10.1038/ngeo889 (2010).
20 Cumming, V. M., Poulton, S. W., Rooney, A. D. & Selby, D. Anoxia in the terrestrial environment during the late Mesoproterozoic. *Geology* **41**, 583-586, doi:10.1130/g34299.1 (2013).
21 Doyle, K. A., Poulton, S. W., Newton, R. J., Podkovyrov, V. N. & Bekker, A. Shallow water anoxia in the Mesoproterozoic ocean: Evidence from the Bashkir Meganticlinorium, Southern Urals. *Precambrian Research* **317**, 196-210, doi:10.1016/j.precamres.2018.09.001 (2018).
22 Clarkson, M. O., Poulton, S. W., Guilbaud, R. & Wood, R. A. Assessing the utility of Fe/Al and Fe-speciation to record water column redox conditions in carbonate-rich sediments. *Chemical Geology* **382**, 111-122, doi:10.1016/j.chemgeo.2014.05.031 (2014).
23 Ruttenberg, K. C. Development of a sequential extraction method for different forms of phosphorus in marine sediments. *Limnol. Oceanogr.* **37**, 1460-1482 (1992).
24 Thompson, J. *et al.* Development of a modified SEDEX phosphorus speciation method for ancient rocks and modern iron-rich sediments. *Chemical Geology* **524**, 383-393 (2019).
25 Strickland, J. D. H. & Parsons, T. R. A practical handbook of seawater analysis. *(2nd edition), Fisheries Research Board of Canada, Ottawa, Bulletin* **167**, 45-64 (1972).
26 Alcott, L. J., Mills, B. J. W. & Poulton, S. W. Stepwise Earth oxygenation is an inherent property of global biogeochemical cycling. *Science* **366**, 1333-1337 (2019).
27 Slomp, C. P. & Van Cappellen, P. The global marine phosphorus cycle: sensitivity to oceanic circulation. *Biogeosciences* **4**, 155-171 (2007).
28 Tsandev, I., Slomp, C. P. & Van Cappellen, P. Glacial-interglacial variations in marine phosphorus cycling: Implications for ocean productivity. *Global Biogeochemical Cycles* **22** (2008).
29 Tsandev, I. & Slomp, C. P. Modelling phosphorus cycling and carbon burial during Cretaceous Oceanic Anoxic Events. *Earth and Planetary Science Letters* **286**, 71-79 (2009).
30 Kasting, J. F. What caused the rise of atmospheric O_2. *Chemical Geology* **362**, 13-25 (2013)
31 Habicht, K. S., Gade, M., Thamdrup, B., Berg, P. & Canfield, D. E. Calibration of sulfate levels in the Archean ocean. *Science* **298**, 5602 (2002)
32 Zhao, M., Zhang, S., Tarhan, L. G., Reinhard, C. T. & Planavsky, N. The role of clacium in regluating marine phosphrous burial and atmospheric oxygenation. *Nature Communications* **11** (2020)
33 Ruttenberg, K. C. & Berner, R. Authigenic apatite formation and burial in sediments from non-upwelling continental margin environments. *Geochim. Cosmochim. Acta*. **57** (1993)
34 Ingall, E. D. & Van Cappellen, P. Relation between sedimentation rate and burial of phosphorus and organic carbonin marine sediments. *Geochim. Cosmochim. Acta*. **54**, 373-386 (1990)
35 Bergman, N. M., Lenton, T. M. & Watson, A. J. COPSE: A new model of biogeochemical cycling over Phanerozoic time. *American Journal of Science* **304**, 397-437 (2004).
36 Creveling, J. R. *et al.* Phosphorus sources for phosphatic Cambrian carbonates. *Geological Society of America Bulletin* **126**, 145-163, doi:10.1130/b30819.1 (2014).
37 Wignall, P. B. & Newton, R. J. Pyrite framboid diameter as a measure of oxygen deficiency in ancient mudrocks. *American Journal of Science* **298**, 537-552 (1998).
38 Farquhar, J. *et al.* Pathways for Neoarchean pyrite formation constrained by mass-independent sulfur isotopes. *PNAS* **110**, 17638-17643 (2013).
39 Kendall, B. et al. Pervasive oxygenation along late Archaean ocean margins. Nature Geoscience **3**, 647-652 (2010).
40 Hao, J., Knoll, A. H., Huang, F., Hazen, R. M. & Daniel, I. Cycling phosphorus on the Archean Earth: Part I. Continental weathering and riverine transport of phosphorus. *Geochimica et Cosmochimica Acta* **273**, 70-84 (2020).

41 Reinhard, C. T., Planavsky, N. J., Olson, S. L., Lyons, T. W. & Erwin, D. H. Earth's oxygen cycle and the evolution of animal life. *Proc Natl Acad Sci U S A* **113**, 8933-8938, doi:10.1073/pnas.1521544113 (2016).
42 Krissansen-Totton, J., Arney, G. N. & Catling, D. C. Constraining the climate and ocean pH of the early Earth with a geological carbon cycle model. *PNAS* **115**, 16 (2018)

Table S4 Analytical data including major element concentrations, iron speciation, C_{org}, and P phases. ND = not determined. BD = below detection (0.95 ppm).

GTF01 - Proximal Koegas Subgroup drill core									
Depth(m)	Al (wt%)	Fe_T (wt%)	Fe_{HR}/Fe_T	Fe_{Py}/Fe_{HR}	Fe_T/Al	C_{org} (wt%)	P_T (ppm)	P_{reac} (ppm)	P_{org} (ppm)
328.45	0.97	24.39	0.48	0.00	25.03	0.065	115	ND	ND
327.50	0.63	26.75	0.66	0.00	42.19	0.047	78	ND	ND
325.10	0.56	32.81	0.75	0.00	58.90	0.037	167	ND	ND
323.00	0.38	24.69	0.69	0.00	65.29	0.039	182	ND	ND
322.45	0.16	21.13	0.78	0.00	129.25	0.022	336	ND	ND
321.90	1.19	25.57	0.52	0.00	21.49	0.035	285	ND	ND
318.95	4.05	19.15	0.20	0.01	4.72	0.044	431	ND	ND
316.30	5.45	14.77	0.14	0.03	2.71	0.043	533	ND	ND
313.60	5.63	13.37	0.12	0.04	2.37	0.041	665	ND	ND
309.75	6.24	6.06	0.25	0.06	0.97	0.065	437	ND	ND
307.30	6.08	10.93	0.26	0.03	1.80	0.074	464	ND	ND
304.05	6.44	8.12	0.24	0.04	1.26	0.066	526	ND	ND
301.45	5.97	8.54	0.23	0.04	1.43	0.084	388	ND	ND
298.40	6.83	10.31	0.16	0.04	1.51	0.040	304	ND	ND
295.30	6.30	10.23	0.19	0.02	1.63	0.049	379	ND	ND
291.85	5.61	11.14	0.32	0.03	1.99	0.067	382	ND	ND
289.00	7.13	5.91	0.24	0.05	0.83	0.056	451	ND	ND
287.30	5.52	7.63	0.28	0.05	1.38	0.057	280	ND	ND
284.00	2.88	21.40	0.21	0.01	7.43	0.036	339	ND	ND
281.80	0.17	26.21	0.74	0.00	156.07	0.036	202	ND	ND
280.70	0.12	21.56	0.63	0.00	173.75	0.040	87	ND	ND
276.90	0.23	34.57	0.72	0.00	150.52	0.032	204	ND	ND
273.30	0.31	31.17	0.74	0.00	100.78	0.052	122	ND	ND
269.95	0.20	24.16	0.70	0.00	118.35	0.036	113	ND	ND
266.05	0.51	28.62	0.68	0.00	56.01	0.050	125	ND	ND
262.60	0.27	32.57	0.56	0.00	119.75	0.055	150	ND	ND
260.10	0.25	31.12	0.78	0.00	125.08	0.038	118	ND	ND
256.80	0.27	28.03	0.62	0.00	103.09	0.017	110	ND	ND
252.55	0.34	26.20	0.64	0.00	76.19	0.036	204	ND	ND
248.80	0.38	21.27	0.77	0.00	55.63	0.065	188	ND	ND
244.80	0.80	22.97	0.73	0.00	28.59	0.068	228	ND	ND
242.90	0.40	24.83	0.79	0.01	61.48	0.067	250	ND	ND
240.00	2.56	16.74	0.33	0.01	6.53	0.114	313	ND	ND
238.00	3.37	17.76	0.61	0.01	5.27	0.113	345	ND	ND
234.00	5.53	7.72	0.33	0.03	1.40	0.060	320	ND	ND
231.00	5.67	10.78	0.35	0.02	1.90	0.056	357	ND	ND
230.25	4.96	7.06	0.37	0.04	1.42	0.061	356	ND	ND
229.40	4.69	13.88	0.56	0.00	2.96	0.080	427	ND	ND
227.60	4.80	14.89	0.30	0.01	3.10	0.052	387	ND	ND
225.00	4.55	11.91	0.43	0.01	2.62	0.044	322	ND	ND
222.90	2.12	16.09	0.44	0.00	7.59	0.037	281	ND	ND
219.60	6.11	10.81	0.31	0.02	1.77	0.060	437	ND	ND
216.45	6.13	15.27	0.38	0.01	2.49	0.053	649	ND	ND
215.50	6.62	14.97	0.30	0.02	2.26	0.037	554	ND	ND
212.15	6.94	10.68	0.17	0.04	1.54	0.035	465	ND	ND
209.20	4.16	13.96	0.40	0.01	3.36	0.041	369	ND	ND
202.85	6.70	14.52	0.36	0.01	2.17	0.054	657	ND	ND
199.10	6.79	11.32	0.28	0.02	1.67	0.052	564	ND	ND
196.30	6.51	9.33	0.33	0.03	1.43	0.047	466	ND	ND
193.00	7.00	9.94	0.21	0.04	1.42	0.050	512	ND	ND
188.40	6.37	10.01	0.30	0.08	1.57	0.037	575	ND	ND

184.50	7.59	10.10	0.18	0.05	1.33	0.049	540	ND	ND
181.20	7.25	13.86	0.26	0.02	1.91	0.058	558	ND	ND
178.50	5.48	3.86	0.46	0.05	0.70	0.038	339	ND	ND
178.10	5.81	9.76	0.43	0.13	1.68	0.033	816	ND	ND
172.50	5.65	10.87	0.35	0.01	1.92	0.031	270	ND	ND
170.30	4.57	9.82	0.45	0.02	2.15	0.036	362	ND	ND
166.00	4.55	9.53	0.46	0.10	2.09	0.028	654	ND	ND
164.00	3.95	3.86	0.41	0.08	0.98	0.033	238	ND	ND
159.90	6.79	14.35	0.38	0.02	2.11	0.031	615	ND	ND
151.90	5.71	9.52	0.36	0.03	1.67	0.032	503	ND	ND
148.90	5.79	13.28	0.37	0.04	2.30	0.040	528	ND	ND
144.60	4.89	11.34	0.41	0.05	2.32	0.025	509	ND	ND
141.15	5.53	10.67	0.36	0.02	1.93	0.031	441	ND	ND
137.30	6.25	12.77	0.35	0.01	2.04	0.040	432	ND	ND
133.90	5.39	11.01	0.28	0.03	2.04	0.045	413	ND	ND
129.65	6.17	14.27	0.27	0.02	2.31	0.024	443	ND	ND
126.65	5.91	10.95	0.24	0.02	1.85	0.051	430	ND	ND
122.80	5.53	13.76	0.29	0.02	2.49	0.039	355	ND	ND
120.05	3.63	16.65	0.32	0.02	4.59	0.033	401	ND	ND
117.60	4.42	18.55	0.36	0.01	4.20	0.052	379	ND	ND
113.50	2.19	17.11	0.30	0.00	7.83	0.035	229	ND	ND
110.90	5.01	11.43	0.37	0.02	2.28	0.034	353	ND	ND
106.00	4.15	13.39	0.40	0.01	3.22	0.043	424	ND	ND
103.35	4.31	18.54	0.36	0.01	4.30	0.039	410	ND	ND
100.60	5.89	13.01	0.26	0.03	2.21	0.043	542	ND	ND
97.45	5.75	12.55	0.31	0.02	2.18	0.033	367	ND	ND
93.20	5.10	14.09	0.38	0.02	2.76	0.042	421	ND	ND
91.00	5.72	10.28	0.32	0.04	1.80	0.021	406	22	1
88.20	5.57	13.45	0.34	0.02	2.42	0.031	369	36	1
83.50	2.51	10.32	0.74	0.01	4.11	0.025	80	5	BD
76.80	4.11	19.61	0.38	0.01	4.77	0.035	401	23	1
73.60	5.77	16.40	0.36	0.01	2.84	0.034	556	16	1
71.35	2.50	21.43	0.22	0.01	8.58	0.050	274	10	BD
69.45	4.82	16.37	0.26	0.01	3.39	0.035	485	55	2
68.50	0.85	20.45	0.48	0.00	24.18	0.048	150	7	BD
68.10	0.71	17.91	0.51	0.01	25.16	0.022	203	12	2
64.85	0.17	20.60	0.78	0.00	123.11	0.048	91	6	ND
63.00	0.21	8.30	0.73	0.00	40.46	0.043	ND	4	BD
62.00	0.20	33.49	0.61	0.00	167.04	0.030	203	8	ND
60.15	0.24	18.55	0.60	0.00	77.36	0.064	219	9	1
57.25	0.29	26.47	0.69	0.00	92.13	0.015	293	12	2
55.00	1.66	16.68	0.46	0.01	10.03	0.214	105	10	1
52.00	3.63	16.80	0.47	0.00	4.63	0.408	222	22	7
51.05	2.19	18.41	0.56	0.00	8.41	0.369	ND	12	2
49.15	2.36	18.81	0.55	0.00	7.96	0.325	150	20	5
47.50	0.43	17.60	0.62	0.06	40.70	0.130	ND	8	1
46.00	0.14	7.70	0.71	0.01	55.50	0.072	ND	3	BD

GEC01 - Distal Koegas Subgroup drill core

Depth(m)	Al (wt%)	Fe_T (wt%)	Fe_{HR}/Fe_T	Fe_{Py}/Fe_{HR}	Fe_T/Al	C_{org} (wt%)	P_T (ppm)	P_{reac} (ppm)	P_{org} (ppm)
372.60	4.38	15.70	0.35	0.00	3.58	0.033	343	ND	ND
368.50	4.43	18.15	0.18	0.02	4.10	0.024	335	ND	ND
364.20	2.75	26.18	0.14	0.01	9.53	0.027	274	ND	ND

365.55	2.30	27.64	0.20	0.00	12.04	0.020	224	ND	ND
362.70	2.19	23.30	0.23	0.02	10.65	0.030	ND	ND	ND
358.70	2.16	13.81	0.73	0.00	6.40	0.025	242	ND	ND
355.30	1.38	12.26	0.81	0.01	8.91	0.024	ND	ND	ND
352.70	1.17	18.47	0.47	0.00	15.78	0.015	ND	ND	ND
349.80	1.56	30.54	0.36	0.00	19.59	0.031	ND	ND	ND
345.90	1.73	21.71	0.27	0.00	12.54	0.035	ND	ND	ND
343.20	3.35	19.61	0.32	0.01	5.85	0.013	259	ND	ND
340.20	5.98	16.26	0.36	0.01	2.72	0.037	383	ND	ND
337.15	4.59	19.24	0.32	0.01	4.19	0.037	377	ND	ND
334.50	4.64	19.09	0.30	0.01	4.11	0.027	311	ND	ND
330.70	5.39	14.54	0.30	0.02	2.70	0.032	300	ND	ND
327.75	3.15	10.74	0.74	0.01	3.41	0.014	ND	ND	ND
324.40	6.53	13.28	0.32	0.02	2.03	0.029	461	ND	ND
321.25	7.04	12.61	0.17	0.03	1.79	0.047	435	ND	ND
318.00	2.90	16.20	0.56	0.00	5.58	0.017	122	ND	ND
314.50	4.02	18.14	0.42	0.01	4.52	0.028	350	ND	ND
312.00	4.44	18.68	0.32	0.01	4.21	0.022	399	ND	ND
309.30	2.68	21.21	0.38	0.01	7.92	0.019	5350	ND	ND
305.00	2.21	16.19	0.69	0.00	7.32	0.024	152	ND	ND
300.65	4.73	19.59	0.38	0.01	4.14	0.021	334	ND	ND
297.75	5.00	15.65	0.22	0.02	3.13	0.025	413	ND	ND
296.30	1.83	25.97	0.42	0.00	14.22	0.016	1221	ND	ND
295.50	1.27	23.49	0.25	0.00	18.45	0.016	212	ND	ND
291.55	0.50	30.00	0.57	0.00	59.98	0.018	200	ND	ND
282.90	0.63	34.40	0.59	0.00	54.39	0.033	306	ND	ND
280.00	0.79	30.05	0.36	0.00	37.88	0.017	1477	ND	ND
277.45	1.69	31.09	0.42	0.00	18.44	0.018	179	57	20
274.90	0.12	26.06	0.71	0.00	219.06	0.016	140	5	1
271.50	1.13	26.61	0.40	0.03	23.48	0.032	80	15	10
267.40	0.31	24.05	0.67	0.00	78.47	0.013	ND	3	BD
263.60	1.22	38.80	0.44	0.00	31.76	0.021	66	21	1
260.55	1.14	25.89	0.48	0.00	22.70	0.022	ND	13	3
256.50	0.23	27.65	0.53	0.00	118.95	0.015	ND	9	BD
250.00	0.11	22.09	0.08	0.00	206.25	0.025	49	17	BD
246.20	0.68	21.25	1.06	0.00	31.03	0.022	ND	6	BD
242.10	ND	36.30	0.30	0.00	ND	0.043	ND	14	BD
238.40	0.11	12.94	0.88	0.00	116.75	0.044	ND	12	BD
234.10	ND	23.65	0.52	0.00	ND	0.049	ND	18	ND
229.30	ND	21.94	0.76	0.00	ND	0.048	93	10	BD
227.20	0.25	26.93	0.63	0.00	106.03	0.035	74	12	BD
224.00	0.35	31.41	0.45	0.00	89.58	0.074	ND	8	BD
219.30	0.21	26.90	0.74	0.00	130.51	0.073	94	13	BD
215.50	0.52	29.23	0.51	0.00	55.77	0.081	117	11	1
211.25	0.31	27.69	0.07	0.01	88.87	0.093	144	8	1
208.00	0.42	27.94	0.65	0.00	65.78	0.080	95	2	BD
205.20	0.39	25.62	0.48	0.00	66.09	0.069	129	11	1
201.20	0.26	27.60	0.68	0.00	105.34	0.061	209	7	1
197.25	0.54	25.61	0.61	0.00	47.57	0.118	194	8	BD
191.50	6.20	14.80	0.20	0.01	2.39	0.128	395	154	80
186.70	1.32	20.52	0.37	0.00	15.55	0.175	212	35	11
182.60	1.27	26.62	0.42	0.00	20.88	0.190	323	28	4
178.10	0.76	33.85	0.50	0.00	44.74	0.020	543	65	2
175.85	4.53	19.54	0.30	0.00	4.31	0.129	323	72	11

170.95	4.28	20.50	0.29	0.00	4.79	0.140	367	95	37
166.70	3.36	25.47	0.48	0.00	7.58	0.125	242	14	2
159.40	2.10	28.67	0.14	0.00	13.64	0.097	356	150	105
155.10	2.93	29.84	0.17	0.01	10.20	0.079	237	73	33
149.30	0.99	27.21	0.34	0.00	27.53	0.042	392	84	18
145.30	2.04	26.71	0.38	0.00	13.10	0.162	1209	36	1
141.55	0.59	36.96	0.58	0.00	62.36	0.018	509	41	1
135.20	0.17	32.03	0.69	0.00	187.83	0.015	689	100	BD
132.35	0.08	25.17	0.55	0.00	302.20	0.016	125	31	BD
123.00	ND	38.95	0.82	0.00	ND	0.018	225	10	BD
105.60	0.35	36.65	0.61	0.00	105.86	0.013	425	12	BD
98.50	0.33	34.53	0.66	0.00	104.21	0.005	154	ND	ND
96.80	ND	22.79	0.13	ND	ND	0.006	249	ND	ND
91.45	2.78	21.99	0.10	0.01	7.92	0.036	205	ND	ND
87.05	0.50	35.12	0.59	0.00	69.75	0.004	293	ND	ND
84.00	0.43	28.76	0.49	0.00	67.15	0.009	80	ND	ND
79.95	0.68	35.87	0.36	0.00	52.72	0.006	173	ND	ND
77.15	0.32	34.78	0.48	0.00	108.67	0.015	243	ND	ND
72.90	1.60	33.36	0.03	0.05	20.87	0.025	333	ND	ND
71.60	0.88	32.87	0.41	0.00	37.56	0.021	185	ND	ND
69.00	3.13	23.57	0.11	0.01	7.53	0.024	201	ND	ND
64.90	0.61	31.28	0.38	0.00	51.27	0.017	53	ND	ND
64.00	1.55	29.66	0.37	0.00	19.13	0.011	232	ND	ND
62.00	2.10	15.67	1.36	0.00	7.47	0.031	110	ND	ND
54.00	0.59	39.37	0.29	0.00	67.06	ND	1465	ND	ND

GKF01 - Proximal Campbellrand Subgroup drill core

Depth(m)	Al (wt%)	Fe_T (wt%)	Fe_{HR}/Fe_T	Fe_{Py}/Fe_{HR}	Fe_T/Al	C_{org} (wt%)	P_T (ppm)	P_{reac} (ppm)	P_{org} (ppm)
183.50	ND	34.99	0.40	0.00	ND	0.500	ND	145	ND
183.80	0.03	31.28	0.38	0.00	1256.09	0.120	348	ND	ND
184.40	ND	21.75	0.16	0.00	ND	0.080	ND	ND	ND
186.30	1.42	25.51	0.24	0.00	18.01	0.960	553	75	3
187.60	0.37	23.57	0.72	0.02	68.23	1.790	1742	125	ND
188.60	ND	19.43	0.68	0.00	ND	1.040	ND	ND	6
189.60	0.21	15.99	0.09	0.00	88.95	0.250	441	245	6
192.30	1.82	24.79	0.19	0.00	12.88	1.640	366	100	4
193.00	ND	11.78	0.47	0.00	ND	0.300	ND	ND	3
195.05	0.75	11.35	0.32	0.00	14.84	0.130	46	5	2
196.70	0.29	17.76	0.85	0.00	75.71	1.840	1092	35	ND
198.42	ND	13.36	1.04	0.00	ND	1.333	ND	ND	ND
200.11	ND	12.37	1.34	0.00	ND	1.500	ND	ND	ND
201.81	ND	11.38	1.69	0.00	ND	1.667	ND	ND	ND
203.50	ND	10.39	2.10	0.00	ND	1.834	ND	ND	ND
205.20	ND	9.40	2.60	0.00	ND	2.001	ND	ND	ND
206.89	ND	8.41	3.22	0.00	ND	2.168	ND	ND	ND
208.59	ND	7.42	4.00	0.00	ND	2.335	ND	ND	ND
210.28	ND	6.43	5.02	0.00	ND	2.502	ND	ND	ND
211.98	ND	5.44	6.41	0.00	ND	2.669	ND	ND	ND
213.67	ND	4.45	8.43	0.00	ND	2.836	ND	ND	ND
215.37	ND	3.46	11.59	0.00	ND	3.003	ND	ND	ND
217.06	ND	2.47	17.29	0.00	ND	3.170	ND	ND	ND
218.76	ND	1.48	30.60	0.00	ND	3.337	ND	ND	ND
220.45	ND	0.49	97.23	0.00	ND	3.504	ND	ND	ND

228.93	0.08	ND	ND	ND	ND	ND	136	7	2
264.00	7.08	4.86	0.54	0.69	0.65	2.460	948	76	45
264.40	ND	4.01	0.95	0.87	ND	5.400	ND	ND	ND
265.00	ND	6.31	0.96	0.91	ND	6.340	ND	ND	ND
265.10	2.65	13.33	0.87	0.89	4.53	4.360	210	15	7
265.20	4.13	9.90	0.79	0.88	2.19	3.090	647	43	10
265.40	3.83	8.61	0.99	0.93	2.12	2.880	424	34	21
265.50	5.66	5.19	0.92	0.83	0.88	3.640	792	83	27
265.70	ND	2.26	0.88	0.86	ND	2.500	ND	ND	ND
268.30	ND	2.94	0.99	0.92	ND	8.140	ND	ND	ND
269.10	6.21	3.67	0.93	0.84	0.57	7.020	469	288	24
274.10	ND	2.74	0.95	0.85	ND	8.640	ND	ND	ND
277.00	0.84	12.13	0.99	0.87	13.61	1.940	89	5	4
280.20	1.30	0.30	0.85	0.29	0.25	3.130	83	66	2
284.00	3.70	13.17	0.64	0.90	3.25	4.530	377	52	5
286.10	1.90	3.56	0.75	0.28	1.79	4.110	207	10	3
286.50	2.61	3.64	0.97	0.37	1.31	4.410	261	11	6
287.30	0.85	4.32	0.75	0.22	4.76	3.130	131	3	2
287.90	1.65	5.90	0.73	0.68	3.31	3.200	294	13	8
289.10	1.71	5.62	0.92	0.43	3.05	2.150	196	11	7
290.00	2.74	5.21	0.78	0.17	1.76	4.240	258	8	3
290.20	1.26	9.21	0.91	0.66	6.80	2.410	159	9	3
291.00	0.82	5.10	0.75	0.09	5.67	1.960	103	3	1
292.00	0.70	5.30	0.95	0.22	6.98	3.440	104	3	1
293.60	1.86	7.37	0.90	0.39	3.69	1.530	86	9	3
293.90	1.26	6.34	0.92	0.29	4.68	3.660	116	6	5
294.70	0.58	5.69	0.71	0.27	9.09	3.360	57	11	3
295.50	0.89	5.63	0.75	0.10	5.81	4.020	91	3	1
296.80	1.77	6.24	0.93	0.07	3.20	3.000	164	12	2
300.60	5.35	7.72	0.45	0.05	1.34	2.190	800	21	5
309.10	ND	ND	ND	0.82	ND	1.440	ND	ND	ND
314.00	0.07	13.43	0.83	0.01	183.56	1.180	54	2	BD
317.50	1.08	10.50	0.90	0.41	8.83	3.570	142	7	2
318.50	2.96	5.99	0.71	0.19	1.84	5.170	130	12	4
319.50	7.20	3.51	0.87	0.29	0.45	6.640	712	27	5
320.30	2.21	6.62	0.93	0.14	2.69	3.620	172	14	3
321.30	1.67	6.49	0.93	0.10	3.55	3.370	167	5	ND
322.30	2.12	5.91	0.74	0.07	2.57	1.990	79	4	ND
322.40	0.80	6.49	0.92	0.04	7.52	1.090	ND	19	4
327.80	5.34	7.48	0.68	0.15	1.27	3.360	202	13	7
337.20	0.63	4.13	0.82	0.39	6.10	4.630	ND	8	4
341.20	1.01	3.40	0.89	0.03	2.95	3.600	ND	10	3
350.20	0.80	2.08	0.92	0.27	2.51	3.920	56	10	7
352.40	0.82	2.36	0.90	0.15	2.72	2.310	65	7	2
354.80	0.80	1.88	0.90	0.17	2.23	2.110	72	3	1
356.00	0.06	2.42	0.80	0.15	38.37	0.990	143	4	1
357.20	0.17	3.20	0.73	0.05	17.97	0.140	ND	9	4
357.90	0.07	3.38	0.64	0.38	50.47	0.220	ND	15	3
358.40	0.02	2.94	0.51	0.10	144.96	0.100	71	5	ND
358.70	0.08	2.08	0.89	0.11	24.63	3.400	186	8	2
361.80	0.42	1.49	0.89	0.19	3.35	2.710	77	12	4
367.40	0.72	1.97	0.88	0.16	2.51	3.020	89	4	3
368.80	0.12	5.45	0.84	0.11	41.64	2.380	123	3	1
377.30	2.71	2.91	0.93	0.74	1.01	1.770	181	15	3

384.50	1.60	3.86	0.82	0.64	2.27	2.170	99	14	3
392.10	0.57	1.61	0.88	0.32	2.87	2.710	217	13	4
400.60	0.90	1.87	0.87	0.25	2.05	2.900	101	11	3
411.70	0.54	1.02	0.88	0.07	1.91	4.580	84	8	1
426.50	0.77	5.90	0.89	0.07	7.28	3.330	382	22	3
438.40	6.07	3.19	0.44	0.18	0.49	1.960	414	23	5
439.70	9.16	5.15	0.60	0.45	0.56	3.130	339	27	10
440.15	8.33	4.49	0.46	0.35	0.51	3.110	288	24	7
441.20	7.66	6.26	0.42	0.21	0.79	2.500	251	23	7
441.80	10.58	5.23	0.41	0.62	0.49	3.550	409	28	10
444.00	12.52	5.26	0.23	0.47	0.40	3.700	340	30	13
445.20	13.22	4.77	0.34	0.66	0.36	3.880	347	90	14
446.10	13.07	4.87	0.24	0.45	0.37	4.760	321	29	13
447.50	11.88	5.49	0.30	0.42	0.45	3.430	297	23	9
448.50	12.43	5.31	0.21	0.47	0.42	3.290	330	26	9
449.90	8.84	5.27	0.47	0.40	0.60	2.290	264	19	7
451.20	10.78	4.66	0.29	0.63	0.43	2.650	287	225	8
452.30	8.95	5.24	0.42	0.27	0.57	2.820	274	31	13
453.60	9.58	3.86	0.34	0.53	0.39	2.230	251	31	18
455.50	5.86	6.37	0.54	0.61	1.07	2.030	318	16	6
456.20	8.36	4.90	0.34	0.33	0.57	2.860	165	14	6
457.10	10.43	3.65	0.32	0.61	0.34	3.110	173	16	5
467.60	1.46	1.38	0.64	0.08	0.91	3.930	107	7	1
474.10	0.68	0.88	0.78	0.06	1.34	4.100	147	8	1
480.30	0.84	1.27	0.86	0.09	1.55	5.510	76	4	BD
492.50	1.11	1.60	0.88	0.02	1.37	2.960	95	6	1
507.10	5.57	2.28	0.54	0.28	0.39	2.820	187	10	3
510.90	0.96	1.12	0.90	0.05	1.22	2.950	118	7	1
523.40	0.67	1.13	0.82	0.02	1.65	3.730	110	6	1
530.80	1.22	0.91	0.76	0.31	0.78	2.690	146	8	BD
544.40	ND	ND	ND	0.04	ND	3.190	ND	ND	1
554.10	4.81	2.02	0.66	0.11	0.44	3.840	174	8	2
569.20	0.38	0.71	0.91	0.02	1.82	3.240	78	5	1
588.90	0.94	1.35	0.89	0.03	1.55	0.380	64	3	1
608.60	5.66	5.02	0.73	0.59	0.91	2.130	239	17	6
628.70	1.21	3.58	0.90	0.17	3.14	0.710	89	6	1
657.80	1.64	0.91	0.82	0.07	0.60	2.750	86	7	1
676.80	12.35	1.65	0.19	0.64	0.15	6.470	321	240	4
705.15	9.68	1.54	0.12	0.36	0.17	3.040	236	171	4
720.30	6.57	1.67	0.39	0.20	0.26	1.500	250	17	3
729.70	7.36	1.56	0.59	0.74	0.23	2.600	260	23	5
756.80	9.69	1.18	0.38	0.52	0.13	3.640	208	163	5
770.60	1.51	4.07	0.25	0.32	2.78	3.200	54	17	13
789.90	1.44	0.63	0.87	0.22	0.46	0.230	128	9	2
815.30	0.34	0.34	0.70	0.08	1.10	2.400	46	5	1
822.60	0.25	0.53	0.90	0.17	2.27	3.360	120	8	1
829.50	9.78	2.65	0.41	0.83	0.28	2.970	293	294	4
830.80	11.99	2.65	0.18	0.67	0.23	2.040	278	187	4
832.10	12.38	2.66	0.19	0.66	0.22	2.200	337	235	4
834.60	11.81	2.88	0.18	0.65	0.25	1.800	268	169	3
835.60	11.91	2.48	0.29	0.72	0.22	2.090	225	137	4
837.20	10.74	2.07	0.15	0.54	0.20	1.740	207	134	3
838.50	6.31	2.00	0.52	0.47	0.32	1.750	228	13	4
841.80	0.13	0.56	0.88	0.00	4.75	2.760	ND	5	BD

855.80	ND	0.62	0.74	0.01	ND	4.240	ND	ND	BD
870.10	0.22	0.77	0.83	0.08	3.71	3.230	93	5	BD
888.30	4.61	1.41	0.70	0.32	0.29	4.790	128	8	1
895.80	ND	3.94	0.90	0.14	ND	0.220	ND	ND	ND
896.40	ND	ND	ND	0.00	ND	1.260	ND	ND	ND
896.90	ND	11.32	0.87	0.00	ND	0.350	ND	ND	ND
917.90	ND	0.58	0.90	0.19	ND	4.780	ND	ND	ND
966.40	1.41	1.28	0.97	0.20	0.86	3.710	133	8	1
982.00	4.21	1.25	0.84	0.59	0.29	3.950	198	13	4
1032.80	ND	0.90	0.93	0.04	ND	4.390	ND	ND	ND
1064.50	0.23	0.77	0.97	0.06	3.13	3.340	410	21	BD
1092.30	2.73	3.39	0.92	0.21	1.19	1.930	103	12	2
1101.40	ND	5.02	0.99	0.03	ND	2.440	ND	ND	ND
1102.60	0.17	3.05	0.78	0.04	17.62	0.280	329	12	1
1104.00	ND	ND	ND	0.01	ND	1.190	ND	ND	ND
1104.20	ND	ND	ND	0.08	ND	3.560	ND	ND	ND
1115.30	0.06	1.76	0.97	0.01	25.76	2.030	298	17	1
1141.80	ND	1.68	0.95	0.31	ND	4.380	ND	ND	ND
1176.50	13.87	1.57	0.09	0.29	0.11	1.900	290	193	4
1179.20	11.55	2.09	0.13	0.24	0.17	2.010	174	113	5
1188.20	ND	1.25	0.96	0.06	ND	3.850	ND	ND	ND
1192.90	10.41	0.98	0.17	0.35	0.09	1.780	152	103	3
1245.70	0.64	1.00	0.99	0.19	1.43	3.100	320	10	1
1270.70	ND	0.85	0.98	0.05	ND	3.010	ND	ND	ND
1281.90	0.40	0.96	0.94	0.14	2.26	1.930	161	9	1
1294.70	0.15	0.86	0.99	0.03	5.36	4.220	160	4	BD
1308.90	ND	3.81	0.31	0.38	ND	1.480	ND	ND	ND
1315.30	0.73	0.74	0.92	0.17	1.04	0.370	ND	21	1
1326.80	10.73	3.00	0.35	0.77	0.27	3.140	301	221	4
1334.10	12.43	2.29	0.17	0.44	0.18	3.400	148	97	4
1336.10	12.02	2.43	0.27	0.62	0.21	4.100	245	144	17
1344.30	6.86	2.75	0.70	0.54	0.40	3.870	106	9	3
1353.30	10.87	2.71	0.20	0.40	0.25	1.900	336	252	19
1354.90	7.92	4.77	0.55	0.76	0.58	2.070	239	69	16
1356.20	3.22	2.74	0.70	0.51	0.83	0.880	125	23	6
1366.80	10.69	2.09	0.39	0.38	0.19	3.890	101	32	2
1381.20	11.98	3.97	0.19	0.34	0.32	2.620	189	88	15
1384.40	12.98	3.37	0.15	0.37	0.26	2.420	209	97	15
1386.50	12.53	3.01	0.19	0.60	0.24	2.150	215	111	14
1395.40	12.49	2.84	0.17	0.41	0.22	2.490	179	114	3
1396.90	13.01	2.58	0.13	0.31	0.20	2.870	137	104	4
1404.60	13.71	1.30	0.25	0.56	0.10	4.050	239	150	3
1413.60	0.85	5.05	0.64	0.62	6.03	0.740	91	7	1
1416.10	1.22	18.46	0.18	0.51	14.88	1.010	77	15	4
1417.70	1.50	14.31	0.23	0.51	9.54	1.460	106	51	3
1418.30	1.92	15.16	0.58	0.80	7.79	0.630	147	100	2
1420.80	1.35	11.46	0.31	0.62	8.60	1.390	111	14	1
1422.10	2.26	25.78	0.21	0.61	9.16	2.380	66	46	9
1425.00	2.85	14.80	0.25	0.56	5.36	2.140	108	12	3
1430.70	0.56	11.54	0.43	0.73	20.88	0.730	46	7	2
1436.30	6.90	8.93	0.75	0.73	1.24	1.570	1242	1097	9
1439.10	7.85	7.39	0.40	0.73	0.91	1.650	449	74	6
1445.20	7.96	3.86	0.24	0.09	0.49	1.240	375	125	4
1445.40	0.23	10.25	0.47	0.71	46.56	0.430	ND	ND	ND

1448.20	7.49	3.93	0.33	0.11	0.53	1.120	337	ND	ND
1451.30	5.55	10.40	0.37	0.09	2.00	0.510	277	ND	ND
1454.30	7.43	7.97	0.14	0.01	1.08	0.650	357	ND	ND
1456.70	7.22	4.46	0.28	0.02	0.62	0.810	526	ND	ND
1462.30	6.96	9.10	0.27	0.06	1.26	0.590	364	ND	ND
1465.50	5.43	9.19	0.15	0.15	1.65	0.450	261	ND	ND
1469.90	5.25	8.92	0.23	0.09	1.63	0.520	238	ND	ND
1474.70	7.29	6.59	0.17	0.06	0.90	0.810	287	ND	ND
1484.40	0.99	1.02	0.58	0.10	1.06	0.220	107	ND	ND
1488.80	ND	0.84	0.59	0.05	ND	0.170	ND	ND	ND
1493.30	0.14	1.09	0.42	0.02	8.22	0.250	ND	ND	ND
1497.50	0.63	5.86	0.54	0.02	1.88	0.410	60	ND	ND

GKP01 - Distal Campbellrand Subgroup drill core

Depth(m)	Al (wt%)	Fe_T (wt%)	Fe_{HR}/Fe_T	Fe_{Py}/Fe_{HR}	Fe_T/Al	C_{org} (wt%)	P_T (ppm)	P_{reac} (ppm)	P_{org} (ppm)
183.10	0.05	25.10	0.07	0.00	504.60	0.020	91	ND	ND
186.60	ND	25.97	0.13	0.00	ND	0.100	ND	ND	ND
188.80	1.95	29.66	0.47	0.00	14.32	1.610	293	ND	ND
190.00	ND	27.84	0.56	0.00	ND	1.300	ND	ND	ND
190.80	1.34	33.22	0.33	0.00	23.79	2.630	188	ND	ND
193.10	ND	25.39	0.21	0.00	ND	1.850	ND	ND	ND
193.70	2.19	28.42	0.07	0.00	11.93	0.110	88	ND	ND
197.20	ND	28.24	0.18	0.00	ND	0.030	ND	ND	ND
198.00	2.62	25.52	0.05	0.00	9.03	0.060	209	ND	ND
199.30	ND	25.50	0.71	0.00	ND	0.030	ND	ND	ND
204.00	1.33	33.56	0.60	0.00	24.37	2.690	1285	ND	ND
205.50	ND	51.99	0.29	0.00	ND	0.040	ND	ND	ND
205.60	0.05	26.58	0.05	0.00	526.59	0.020	ND	ND	ND
208.40	ND	34.59	0.39	0.00	ND	0.020	ND	ND	ND
210.90	1.33	31.32	0.59	0.00	22.62	0.660	615	ND	ND
212.00	ND	31.60	0.38	0.00	ND	1.150	ND	ND	ND
213.50	ND	32.17	0.26	0.00	ND	0.310	103	ND	ND
214.90	ND	35.53	0.38	0.00	ND	0.020	ND	ND	ND
219.50	1.82	29.05	0.09	0.00	14.84	0.040	199	ND	ND
220.90	ND	36.41	0.45	0.00	ND	0.050	ND	ND	ND
221.00	0.07	14.73	0.13	0.18	40.55	0.070	ND	ND	ND
221.90	ND	24.96	0.09	0.03	ND	1.240	ND	ND	ND
222.60	0.06	17.29	0.81	0.00	287.43	1.460	1012	ND	ND
223.00	ND	27.80	0.28	0.00	ND	1.380	ND	ND	ND
223.55	0.42	36.37	0.75	0.02	90.44	5.510	937	ND	ND
226.10	1.04	30.28	0.57	0.02	29.46	0.300	4874	ND	ND
226.50	5.73	12.37	0.41	0.02	2.20	1.650	501	ND	ND
227.10	4.58	18.91	0.52	0.05	4.26	1.320	368	ND	ND
227.40	0.08	23.58	0.75	0.00	354.73	0.250	214	ND	ND
228.30	6.81	9.53	0.45	0.05	1.40	1.840	438	ND	ND
230.00	0.11	22.98	0.88	0.00	227.96	0.320	635	ND	ND
231.00	ND	10.73	0.62	0.03	ND	4.120	ND	ND	ND
232.00	5.46	18.90	0.40	0.04	3.54	0.420	356	ND	ND
233.90	7.55	7.61	0.65	0.04	1.00	2.280	348	ND	ND
234.50	4.80	21.97	0.77	0.05	4.47	1.880	635	ND	ND
235.10	3.23	29.23	0.70	0.09	9.11	1.290	288	ND	ND
236.10	6.55	8.59	0.57	0.15	1.30	5.160	631	ND	ND
236.70	0.29	25.75	0.78	0.08	94.53	1.720	191	ND	ND

237.05	6.40	13.65	0.40	0.04	2.10	2.750	471	ND	ND
237.10	0.67	21.13	0.73	0.01	34.00	0.540	1329	ND	ND
237.50	3.76	20.38	0.61	0.05	5.35	2.560	713	ND	ND
238.30	3.74	25.38	0.70	0.08	6.67	1.200	539	ND	ND
238.50	5.15	15.48	0.52	0.03	3.00	1.260	430	ND	ND
239.50	7.57	8.81	0.28	0.04	1.13	2.000	402	ND	ND
239.70	3.14	18.42	0.70	0.01	5.85	1.720	357	ND	ND
240.20	7.62	8.57	0.26	0.04	1.11	2.130	445	ND	ND
240.50	7.45	8.55	0.36	0.02	1.12	2.180	536	ND	ND
241.50	5.73	11.51	0.24	0.36	1.97	2.010	417	ND	ND
242.60	8.03	5.28	0.28	0.10	0.64	2.360	394	ND	ND
243.60	8.02	5.12	0.27	0.12	0.62	2.760	397	ND	ND
244.98	7.99	4.72	0.36	0.29	0.60	2.860	478	ND	ND
245.60	7.83	4.97	0.27	0.18	0.61	2.850	459	ND	ND
246.20	7.54	5.63	0.28	0.26	0.72	3.130	473	102	25
248.00	6.99	8.93	0.37	0.09	1.24	2.990	329	27	14
249.80	4.66	15.43	0.36	0.04	3.05	2.750	522	35	15
255.50	0.30	26.72	0.70	0.00	92.79	0.440	76	6	1
257.90	ND	14.10	0.62	0.04	ND	0.510	ND	ND	ND
258.20	3.33	16.57	0.29	0.03	4.90	2.000	570	18	8
260.00	ND	14.26	0.69	0.02	ND	2.140	ND	ND	ND
260.90	3.09	14.08	0.41	0.11	4.64	1.620	547	33	10
261.20	ND	10.60	0.19	0.05	ND	1.950	ND	ND	ND
262.60	ND	10.22	0.46	0.03	ND	1.720	ND	ND	ND
264.80	2.99	13.95	0.19	0.15	4.57	1.470	490	46	15
266.00	ND	12.42	0.40	0.03	ND	1.810	ND	ND	ND
267.20	3.16	12.46	0.48	0.06	3.73	1.670	530	66	11
269.90	ND	12.39	0.28	0.01	ND	1.530	ND	ND	ND
271.60	1.05	27.67	0.56	0.01	26.19	0.930	347	15	7
274.70	ND	10.73	0.39	0.01	ND	1.530	ND	ND	ND
276.80	4.02	9.17	0.46	0.02	2.22	1.600	452	41	10
277.00	ND	21.30	0.29	0.24	ND	0.910	ND	ND	ND
277.50	3.64	8.40	0.37	0.03	2.19	1.960	384	49	29
283.80	ND	13.18	0.42	0.01	ND	1.810	ND	ND	ND
286.00	2.03	13.07	0.42	0.01	6.13	0.840	281	11	4
291.20	0.20	7.35	0.41	0.02	35.05	0.120	938	20	3
292.50	2.47	12.12	0.56	0.05	4.61	1.710	566	17	5
297.50	1.75	12.04	0.26	0.18	6.63	1.230	514	16	4
301.80	5.27	2.11	0.22	0.25	0.38	2.370	408	154	4
303.90	8.74	1.50	0.20	0.33	0.16	1.890	663	178	27
306.10	4.88	10.11	0.22	0.40	1.88	3.210	466	239	216
307.00	4.40	7.69	0.76	0.62	1.60	3.530	320	20	9
309.00	5.48	3.19	0.79	0.75	0.55	3.570	255	20	9
310.20	5.00	3.76	0.78	0.79	0.70	4.220	383	24	10
311.20	7.16	2.61	0.71	0.71	0.34	3.230	250	17	7
312.50	5.64	4.56	0.41	0.76	0.74	8.700	213	197	30
315.00	6.71	1.77	0.80	0.71	0.25	3.310	488	52	5
316.10	8.70	1.34	0.63	0.60	0.15	4.120	475	106	13
317.10	6.91	2.62	0.85	0.76	0.36	2.560	339	31	7
317.80	2.70	10.88	0.25	0.46	3.79	1.510	1286	67	13
318.00	5.21	1.41	0.75	0.50	0.26	2.320	394	112	4
319.10	4.91	9.57	0.42	0.83	1.85	4.340	285	31	8
320.00	4.65	6.76	0.28	0.75	1.41	4.630	207	104	11
321.10	3.08	3.77	0.92	0.81	1.16	3.200	228	16	5

321.90	6.05	2.64	0.63	0.72	0.41	6.490	349	94	5
324.70	ND	3.77	0.82	0.44	ND	5.320	ND	ND	ND
328.30	0.70	6.02	0.72	0.12	8.41	0.880	62	7	2
332.70	ND	1.88	0.52	0.14	ND	0.140	ND	ND	ND
337.00	0.37	5.32	0.75	0.19	13.24	4.640	125	7	2
361.90	1.81	3.51	0.65	0.33	1.77	4.100	145	12	4
369.10	ND	5.09	0.49	0.45	ND	3.770	ND	ND	ND
371.00	5.22	2.56	0.80	0.61	0.47	2.390	307	16	5
403.00	ND	2.08	0.66	0.02	ND	2.300	ND	ND	ND
445.60	9.64	1.19	0.34	0.79	0.11	0.360	103	33	5
482.80	ND	5.40	0.32	0.18	ND	2.790	ND	ND	ND
484.95	10.37	5.57	0.33	0.16	0.48	2.860	457	23	6
486.70	ND	9.27	0.53	0.08	ND	1.930	ND	ND	ND
490.00	9.44	11.11	0.50	0.14	1.04	2.300	328	17	4
490.70	ND	9.89	0.60	0.07	ND	2.060	ND	ND	ND
491.95	ND	8.56	0.42	0.05	ND	2.050	ND	ND	ND
495.90	12.31	2.43	0.31	0.51	0.18	2.920	272	26	4
497.20	ND	2.77	0.26	0.27	ND	3.900	ND	ND	ND
499.40	ND	1.73	0.87	0.06	ND	3.730	ND	ND	ND
503.50	2.09	3.08	0.83	0.42	1.29	3.640	140	8	2
503.90	ND	20.53	0.08	0.54	ND	1.750	ND	ND	ND
509.10	1.12	2.03	0.83	0.76	8.78	3.660	38	20	15
592.90	1.78	1.16	0.77	0.23	0.59	3.940	93	8	4
624.50	0.08	0.75	0.90	0.00	6.71	2.680	32	6	1
637.10	ND	2.05	0.27	0.75	ND	2.000	ND	ND	ND
637.80	ND	1.88	0.16	0.84	ND	2.040	ND	ND	ND
638.40	11.51	2.08	0.34	0.94	0.16	2.080	208	141	5
639.20	ND	2.56	0.38	0.91	ND	2.010	ND	ND	ND
640.00	ND	1.64	0.08	0.64	ND	1.850	ND	ND	ND
640.60	6.99	1.80	0.12	0.75	0.23	2.200	173	122	5
649.20	ND	2.73	0.57	0.54	ND	4.800	ND	ND	ND
679.50	0.31	0.80	0.82	0.00	2.17	0.130	ND	10	1
722.10	0.14	0.86	0.92	0.05	5.41	3.460	ND	19	1
779.60	ND	0.99	0.98	0.07	ND	5.120	ND	ND	ND
816.70	0.09	1.02	0.53	0.00	10.07	2.690	ND	4	BD
864.70	ND	1.29	0.15	0.65	ND	3.840	ND	ND	ND
905.60	0.33	1.05	0.86	0.06	2.77	3.780	182	7	1
946.50	ND	0.93	0.86	0.06	ND	4.870	ND	ND	ND
972.00	0.29	1.57	0.84	0.28	5.12	0.290	1452	54	2
982.00	ND	1.77	0.39	0.93	ND	3.270	ND	ND	ND
992.10	3.71	1.59	0.89	0.39	0.38	4.000	113	15	4
999.90	ND	0.93	0.42	0.99	ND	3.780	ND	ND	ND
1010.10	3.69	3.87	0.77	0.31	0.94	2.080	124	7	3
1016.30	ND	2.03	0.06	0.22	ND	2.400	ND	ND	ND
1017.70	11.53	2.53	0.19	0.69	0.20	1.740	166	108	5
1019.30	ND	2.39	0.12	0.65	ND	2.410	ND	ND	ND
1020.05	13.63	2.48	0.09	0.50	0.19	1.980	528	280	4
1024.05	ND	1.82	0.95	0.16	ND	3.630	ND	ND	ND
1024.90	3.02	2.18	0.92	0.16	0.75	3.630	136	17	1
1026.20	ND	1.98	0.93	0.55	ND	3.910	ND	ND	ND
1027.70	ND	3.55	0.38	0.91	ND	2.080	ND	ND	ND
1028.30	14.11	1.83	0.17	0.36	0.15	2.390	219	132	4
1028.90	ND	2.16	0.15	0.68	ND	2.290	ND	ND	ND
1029.00	12.81	2.03	0.23	0.68	0.19	2.140	241	127	4

1029.70	ND	4.58	0.09	0.46	ND	1.880	ND	ND	ND
1029.90	ND	2.18	0.53	0.82	ND	6.980	ND	ND	ND
1030.80	ND	2.79	0.12	0.45	ND	3.220	ND	ND	ND
1032.80	11.38	3.04	0.16	0.47	0.28	5.530	214	119	5
1033.60	ND	2.79	0.69	0.55	ND	2.220	ND	ND	ND
1035.90	14.02	1.62	0.35	0.80	0.12	3.580	225	143	3
1035.90	ND	1.47	0.31	0.75	ND	2.870	ND	ND	ND
1036.80	ND	6.96	0.19	0.24	ND	0.650	ND	ND	ND
1038.30	ND	1.46	0.90	0.37	ND	1.940	ND	ND	ND
1039.20	1.33	1.26	0.90	0.26	0.93	1.570	57	19	BD
1040.20	1.97	1.51	0.92	0.42	0.79	2.740	62	6	2
1041.20	4.92	1.75	0.85	0.35	0.37	1.890	90	5	2
1041.60	0.67	1.39	0.83	0.25	1.94	1.500	37	6	1
1042.30	1.38	10.07	0.21	0.51	8.25	0.820	80	9	3
1043.00	1.31	24.39	0.97	0.90	19.58	1.010	72	9	5
1044.60	0.83	21.64	0.14	0.43	27.13	2.860	60	8	5
1046.20	0.89	21.03	0.05	0.68	24.89	2.740	82	7	3
1046.60	0.81	16.68	0.18	0.10	20.97	3.400	45	6	2
1047.20	2.48	5.25	0.42	0.59	2.53	2.160	200	8	2
1048.20	2.36	27.68	0.30	0.73	11.88	1.070	72	11	4
1048.30	8.08	6.97	0.19	0.71	0.89	5.250	230	148	7
1049.50	1.21	18.33	0.17	0.56	15.97	4.230	60	9	4
1050.40	0.99	6.71	0.27	0.52	7.68	0.910	45	8	2
1050.90	1.05	7.89	0.99	0.86	7.72	2.910	53	7	2
1051.30	2.59	20.01	0.14	0.65	8.16	1.240	56	6	3
1051.50	3.44	16.41	0.12	0.39	5.31	1.680	72	8	4
1051.90	0.92	12.38	0.23	0.63	15.14	1.690	29	5	ND
1052.10	1.62	18.94	0.20	0.71	12.54	1.700	57	11	5
1052.70	2.20	10.65	0.96	0.88	4.86	3.110	89	7	3
1054.10	3.41	10.76	0.66	0.82	3.25	1.250	544	19	3
1054.20	ND	2.32	0.73	0.85	ND	0.350	ND	ND	ND
1056.10	0.81	5.43	0.41	0.63	7.69	0.730	39	21	1
1059.10	11.20	2.03	0.05	0.64	0.19	0.540	124	83	2
1059.20	8.58	1.74	0.38	0.51	0.22	2.350	190	67	7
1060.10	7.33	5.87	0.62	0.79	0.80	2.630	345	33	3
1061.00	7.26	5.50	0.50	0.79	0.88	3.950	507	94	6
1062.00	7.30	5.04	0.59	0.67	0.71	1.490	1682	41	9
1062.30	7.16	4.52	0.54	0.69	0.71	1.800	1091	ND	ND
1062.90	5.18	14.81	0.20	0.63	3.19	1.000	1510	37	10
1063.40	6.82	4.07	0.50	0.31	0.64	1.700	703	24	5
1063.50	7.01	5.46	0.56	0.44	0.83	1.710	660	21	5
1064.10	8.86	3.53	0.25	0.30	0.42	1.880	538	87	5
1064.20	7.95	4.65	0.40	0.53	0.70	0.690	861	27	8
1074.20	8.60	11.03	0.09	0.10	1.54	0.220	278	88	7
1077.20	6.05	9.58	0.26	0.12	1.78	0.450	267	23	6
1080.50	6.59	8.43	0.22	0.09	1.48	0.430	340	29	8
1084.70	6.71	8.81	0.27	0.23	1.48	0.520	304	21	6
1091.80	ND	5.52	0.23	0.22	ND	0.720	ND	ND	ND
1092.50	8.20	4.72	0.23	0.09	0.60	0.930	683	176	7
1115.60	8.01	6.68	0.25	0.30	0.95	0.510	482	70	8
1121.10	ND	8.29	0.12	0.31	ND	0.660	ND	ND	ND
1129.20	4.29	10.42	0.18	0.23	2.80	0.350	236	27	4
1136.00	4.34	12.95	0.27	0.18	3.45	0.430	238	20	5
1143.70	6.61	11.19	0.20	0.10	2.03	0.470	304	31	14

1150.80	ND	12.24	0.14	0.17	ND	0.570	ND	ND	ND
1162.80	3.51	14.52	0.10	0.40	4.90	0.330	230	57	7
1173.30	3.02	18.46	0.21	0.03	7.51	0.410	214	10	3
1182.20	ND	13.66	0.20	0.04	ND	0.480	ND	ND	ND
1189.80	8.31	7.79	0.18	0.39	1.22	0.500	369	42	9
1194.20	8.83	6.43	0.13	0.09	0.89	0.610	369	128	6
1199.20	ND	7.32	0.17	0.37	ND	0.680	ND	ND	ND
1209.60	9.55	1.04	0.56	0.45	0.14	1.670	619	114	6
1214.30	7.42	9.39	0.18	0.23	1.55	0.670	441	96	7
1224.30	ND	4.55	0.10	0.30	ND	0.620	ND	ND	ND
1228.50	8.22	8.15	0.18	0.46	1.17	0.520	514	149	6
1229.60	7.41	5.29	0.15	0.42	0.88	0.600	476	173	5
1235.20	ND	5.02	0.21	0.31	ND	0.540	ND	ND	ND
1244.60	8.19	5.26	0.22	0.45	0.78	0.800	675	67	7
1247.45	8.13	5.24	0.20	0.24	0.76	0.520	1148	48	7
1251.70	ND	4.04	0.18	0.23	ND	0.560	ND	ND	ND
1255.10	9.78	7.47	0.14	0.38	0.90	0.670	559	208	7
1261.10	9.06	4.77	0.15	0.22	0.61	0.710	507	169	5
1265.50	ND	4.18	0.13	0.41	ND	0.670	ND	ND	ND
1267.90	8.59	4.27	0.24	0.64	0.56	0.660	487	163	13
1270.10	8.21	3.67	0.14	0.36	0.52	0.570	437	173	6
1272.60	ND	4.15	0.09	0.17	ND	0.420	ND	ND	ND
1275.80	9.82	6.03	0.14	0.15	0.74	0.730	524	180	8
1277.00	9.69	6.59	0.12	0.29	0.82	0.610	414	158	7
1280.10	ND	6.01	0.20	0.49	ND	0.700	ND	ND	ND
1281.60	10.34	5.85	0.22	0.67	0.64	0.900	413	177	9
1281.85	9.90	4.73	0.16	0.40	0.57	0.830	363	164	6
1282.70	ND	5.44	0.12	0.10	ND	1.020	ND	ND	ND
1293.60	9.94	13.54	0.10	0.01	1.49	1.010	479	199	6
1300.90	12.50	8.52	0.15	0.30	0.79	0.700	698	213	5
1302.45	ND	13.08	0.24	0.30	ND	0.530	ND	ND	ND
1306.60	5.12	6.47	0.15	0.11	1.50	0.210	441	175	ND

512

513

514

515